remote sensing

MDPI

Article

A Multi-Model Framework Based on Remote Sensing to Assess Land Degradation in Rural Areas

Federica D'Acunto [1], Olena Dubovyk [2], Nikhil Raghuvanshi [2], Francesco Marinello [1], Filippo Iodice [3] and Andrea Pezzuolo [1,*]

[1] Department of Land, Environment, Agriculture and Forestry, University of Padova, 35020 Legnaro, Italy; federica.dacunto@studenti.unipd.it (F.D.); francesco.marinello@unipd.it (F.M.)
[2] Institute of Geography, University of Hamburg, 20146 Hamburg, Germany; olena.dubovyk@uni-hamburg.de (O.D.); nikhil.raghuvanshi@studium.uni-hamburg.de (N.R.)
[3] Uptoearth GmbH, 64293 Darmstadt, Germany; filippo.iodice@uptoearth.eu
* Correspondence: andrea.pezzuolo@unipd.it

Highlights

What are the main findings?

- The application of standard approaches for monitoring land degradation to the Italian rural areas revealed several limitations;
- A new model, specifically tailored to the characteristics of the study area, was developed and tested.

What is the implication of the main finding?

- Since land degradation is highly context-specific, the monitoring approach must also be adapted accordingly;
- While context-specific methods may lead to a proliferation of approaches rather than standardization, they enable more targeted analysis and interventions.

Abstract

Land degradation is a complex and context-specific phenomenon with significant implications for rural areas, where agricultural and livestock activities intersect with natural ecosystem processes. Despite growing efforts to monitor land degradation, the absence of standardized methodologies limits the comparability of results and the implementation of coherent mitigation strategies. This study introduces RURALIS, a multi-model framework, based on remote sensing, specifically designed to assess land degradation in the rural areas of Italy. Drawing on the structure and outputs of three existing models, RURALIS adopts a model-learning approach. A Random Forest classifier is then employed to compare outputs from all models and identify areas of severe degradation across all models. The analysis reveals that approximately 2.34 million hectares (13.6%) of Italy's rural lands are severely degraded, with hotspots in northern Puglia, Sicilia, and parts of northern Italy. The model demonstrates strong classification performance and provides a flexible, high-resolution tool that leverages the shared foundation of remote sensing to deliver spatially detailed, decision-ready outputs for rural land management.

Keywords: agriculture; rural areas; environmental modelling; spatial analysis

check for updates

Academic Editors: Zhenwei Shi, Xiaoyan Lu, Yuting Wan, Zhuo Zheng and Ce Zhang

Received: 1 August 2025
Revised: 14 September 2025
Accepted: 20 September 2025
Published: 24 September 2025

Citation: D'Acunto, F.; Dubovyk, O.; Raghuvanshi, N.; Marinello, F.; Iodice, F.; Pezzuolo, A. A Multi-Model Framework Based on Remote Sensing to Assess Land Degradation in Rural Areas. *Remote Sens.* **2025**, *17*, 3276. https://doi.org/10.3390/rs17193276

Copyright: © 2025 by the authors. Licensee MDPI, Basel, Switzerland. This article is an open access article distributed under the terms and conditions of the Creative Commons Attribution (CC BY) license (https://creativecommons.org/licenses/by/4.0/).

1. Introduction

Land degradation (LD) refers to the "reduction or loss of the biological or economic productivity and complexity of rainfed cropland, irrigated cropland, or range, pasture, forest and woodlands resulting from land uses or from a process or combination of processes" [1]. In rural contexts, it is more specifically defined as "degradation of soil quality due to which agricultural land in particular is unproductive as a consequence of the loss of ability to produce crops and biomass caused by multiple factors that limit or inhibit the productive, regulatory and utilitarian functions as well as eco-system services that a natural soil can offer" [2].

LD is a complex, context-specific phenomenon [3] influenced by geographical, ecological, climatical, and socio-economic factors [4], with estimated global economic losses ranging from USD 6.3 to 10.6 trillion annually [5].

These figures highlight the importance of monitoring LD for defining adequate mitigation measures [6], especially in rural areas that play a key role in providing ecosystem services. However, rural areas can also be sources of ecosystem "disservices", such as those caused by intensive agricultural practices or land abandonment, leading to trade-offs in biodiversity, and in the regulatory and cultural functions of these ecosystems [7,8].

Despite its urgency, monitoring LD presents several challenges. One of the main obstacles is the lack of a standardized methodology. Although several attempts to establish unified approaches, differences in data availability—type, scale, temporal coverage, and spatial resolution—combined with the need to contextualize the analysis to the target area, have resulted in the proliferation of multiple methodologies. Nevertheless, a shared feature across all approaches is the acknowledgment of the central role of remote sensing in monitoring LD [9].

Remote sensing, and especially earth observation satellites, in fact, play a crucial role in analyzing degradation dynamics, offering advantages such as lower costs, broad accessibility, high accuracy, and extensive spatial, temporal, and spectral coverage. The open access nature of many satellite missions, alongside the development of user-friendly platforms, such as Google Earth Engine (GEE), which facilitates data accessibility, and Trends.Earth, which simplifies LD analysis [10]. Furthermore, technological advancements have significantly improved spatial resolution, enabling the production of LD maps at scales ranging from 10 km [11] to 10 m [12]. This has expanded the potential for analysis at various scales—global [13], continental [14], regional [15]—and even at local levels such as cities or districts [16,17]. Perhaps the most critical advantage of satellite data is the possibility to perform historical analysis and trends, which can be used to assess an average time period of 20 years, and, in some cases, over five decades [18,19].

Based on a previous review analysis [9], available remote sensing technologies, indicators and models to study LD in rural areas were investigated. Findings from that work showed that while Sentinel missions offer higher-resolution data compared to Landsat and MODIS, they remain underutilized due to limitations in time series availability. Vegetation indices are the most frequently used indicators; however, they risk oversimplification, as vegetation degradation is only one component of LD.

Furthermore, no single model can comprehensively capture LD across different scales and ecosystems; existing models vary in their goals and capacity. Some, such as MEditerranean Desertification And Land USe (MEDALUS), initially developed for the Mediterranean area [20], and the Risk Assessment of Land Degradation (RALDE) model, designed specifically for Iran [21], focus on identifying areas at risk. Other models assess space–temporal decline, such as the Universal Soil Loss Equation (USLE) and the Revised Universal Soil Loss Equation (RUSLE), both combined in research by AbdelRahman et al. [22] or the Carnegie–Ames–Stanford Approach (CASA), employed to assess degradation dy-

namics in Chinese grasslands [23]. Approaches, such as the Geodetector model [24], can help to identify degradation drivers, while machine learning approaches, such as neural networks, are increasingly used for predictive modelling, as seen, for example, in research by Aldabbagh et al. [25].

Another major advantage of satellite data is the possibility to combine or fuse multiple data sources to improve data accuracy. The most notable example is the fusion of Synthetic Aperture Radar (SAR) imagery with optical ones. Nevertheless, due to the complexity of SAR data interpretation, this approach remains underexplored [4]. Promising examples are, for instance, the combination of Sentinel-1 and Sentinel-2 imagery to compute the land-cover change sub-indicator of the Land Degradation Neutrality (LDN) index [26], or their combination to assess tillage and bare soil impacts on agricultural lands and predict Soil Organic Carbon (SOC) variation, another sub-indicator of the LDN index [27].

To further address the complexity of the LD process, researchers have developed composite indexes and integrated models. Examples include the Land Degradation Status Index (LDSI) [28] or the Land Degradation Development Index (LDDI) [11] and models such as the Integrated Desertification Index (IDI) [6]. More recently, new approaches have emphasized the synergistic effects of multiple degradation processes, especially in agricultural landscapes, leading to the development of new tools, such as the Land Multi-Degradation Index (LMI) [5], which captures the complex, interconnected nature of degradation dynamics more comprehensively. The shift towards integrated assessment is especially relevant in national contexts, like that of Italy, where LD processes are influenced by a combination of human and natural factors.

According to the Italian Institute for Environmental Protection and Research (ISPRA), approximately 10% of Italy's territory was at risk of degradation in 2021 [2], a figure that rose to 17.4% in 2024 [29], with southern regions particularly affected [6]. Previous works have highlighted that LD in Italy is associated mainly with unsustainable agricultural management, including land abandonment, and with climate change, which is associated with an unfavorable orography and steep slopes and has been demonstrated to lead to several degradation processes [2,29,30]. According to Panagos et al., about 33% of Italy's total agricultural lands suffer from severe erosion, resulting in annual economic losses of approximately EUR 619 million [31].

At the national level, most scientific studies have focused on individual degradation processes, such as soil erosion [6,32,33], with research typically conducted at regional or local scales [34,35]. These studies often employ specific models to investigate either a single degradation process [30,36,37] or degradation as a whole [38,39], reflecting the fragmented but growing body of knowledge on LD in the Italian context.

The aim of this study is to develop a new remote sensing model—the RURal Areas Land Degradation Indicator System (RURALIS)—for assessing and monitoring LD in rural areas. Its design is the result of an inverse engineering approach, where the three most widely used approaches—MEDALUS [20], LDN index [40] and the Albedo–Vegetation method [41]—were applied to the reference area. The analysis of their strengths and weaknesses served as a propaedeutic step, providing the conceptual foundation for the creation of RURALIS.

The RURALIS model introduces a multi-criteria framework that incorporates key indicators of land and vegetation conditions and human pressures and thus generates a spatially detailed degradation index for rural areas across Italy. The result is a model that offers enhanced spatial resolution, rural-context specificity, and flexibility for application at national and regional or sub-regional scales. While the primary contribution of this study is not to standardize a land degradation methodology, it demonstrates that land degradation is highly context-specific and requires flexible, tailored approaches. This

context-specific perspective allows for a more accurate representation of degradation processes, particularly in rural areas, where agriculture and livestock interact most intensely. In this sense, the RURALIS framework contributes both to a methodological advancement—by integrating remote sensing and multi-model information in a flexible manner—and to monitoring land degradation in landscapes where human and environmental factors are closely intertwined. At the same time, we acknowledge that such an approach may lead to a proliferation of methods, which represents a trade-off between adaptability to local contexts and comparability across studies.

2. Materials and Methods

2.1. Study Area

The study focuses on rural areas in Italy, defined as areas where agricultural and livestock activities take place. To identify rural zones associated with this specific land use, multiple land-cover layers were used to exclude non-rural land uses such as forests, urban zones, water bodies, road networks, and coastal or lagoon areas.

EUCROPMAP [42] (10 m resolution) represented the master layer, as it has been employed to identify lands covered with non-permanent crops (Classes 211, 212, 213, 214, 215, 216, 217, 218, 219, 221, 222, 223, 230, 231, 232, 233, 240, 250, 290 of EUCROPMAP) and grasslands (Class 500 of EUCROPMAP).

From this layer, forested areas were removed using the Forest/Non-Forest map (FNF) from ALOS PALSAR [43] (25 m resolution), while urban areas were excluded using the GHSL Global settlement characteristics dataset (P2023A) (10 m resolution) [44].

Road networks (Classes "railways" and "roads" of OSM) and water bodies (Class "water" of OSM) were extracted from OpenStreetMap (OSM). Lastly, water bodies, coastal, and lagoon areas were further removed using the backscattering reflectance of Sentinel-1 [45] (10 m resolution).

The flowchart below (Figure 1) illustrates the process used to extract the rural areas mask. Only selected categories were retained from EUCROPMAP, while others—specifically Class 300 (woodland and shrubland, including permanent crops)—were excluded and additional ancillary layers were applied. This decision was based on prior experience indicating potential misclassifications in EUCROPMAP, particularly between non-permanent crops and urban areas or roads [46]. Moreover, the permanent crops class included categories beyond the scope of this study. By adopting a multi-layer exclusion strategy rather than a purely inclusion-based approach, classification errors were minimized, thereby improving the spatial accuracy and reliability of the resulting dataset.

All satellite datasets were accessed via GEE [47] and processed using QGIS software (version 3.4.2.0) [48]. To optimize downloading and processing, the national territory was divided into four macro-regions: North, Centre, South, and Islands. The final rural area map was exported as a vector file, dissolved, and split into 32 tiles covering the entire country.

According to this classification, rural areas in Italy cover a total of 17,269,946.95 ha (Figure 2).

2.2. Data Collection and Modelling

The approach developed in this article is based on the implementation and comparison of three existing models for LD for the development of a new one. MEDALUS, LDN and Albedo–Vegetation feature spaces were selected by considering several aspects. First, the degree of application was considered, as all the models represent the most widespread models used to identify areas at risk of degradation or to monitor LD over time. Furthermore, the models have all been applied at a national scale or can potentially also be applied at lower scales [9]. Other criteria include replicability, application, and resolution, as all the

selected models require input datasets that can be easily collected and processed without specific computation capacity, granting the highest resolution possible.

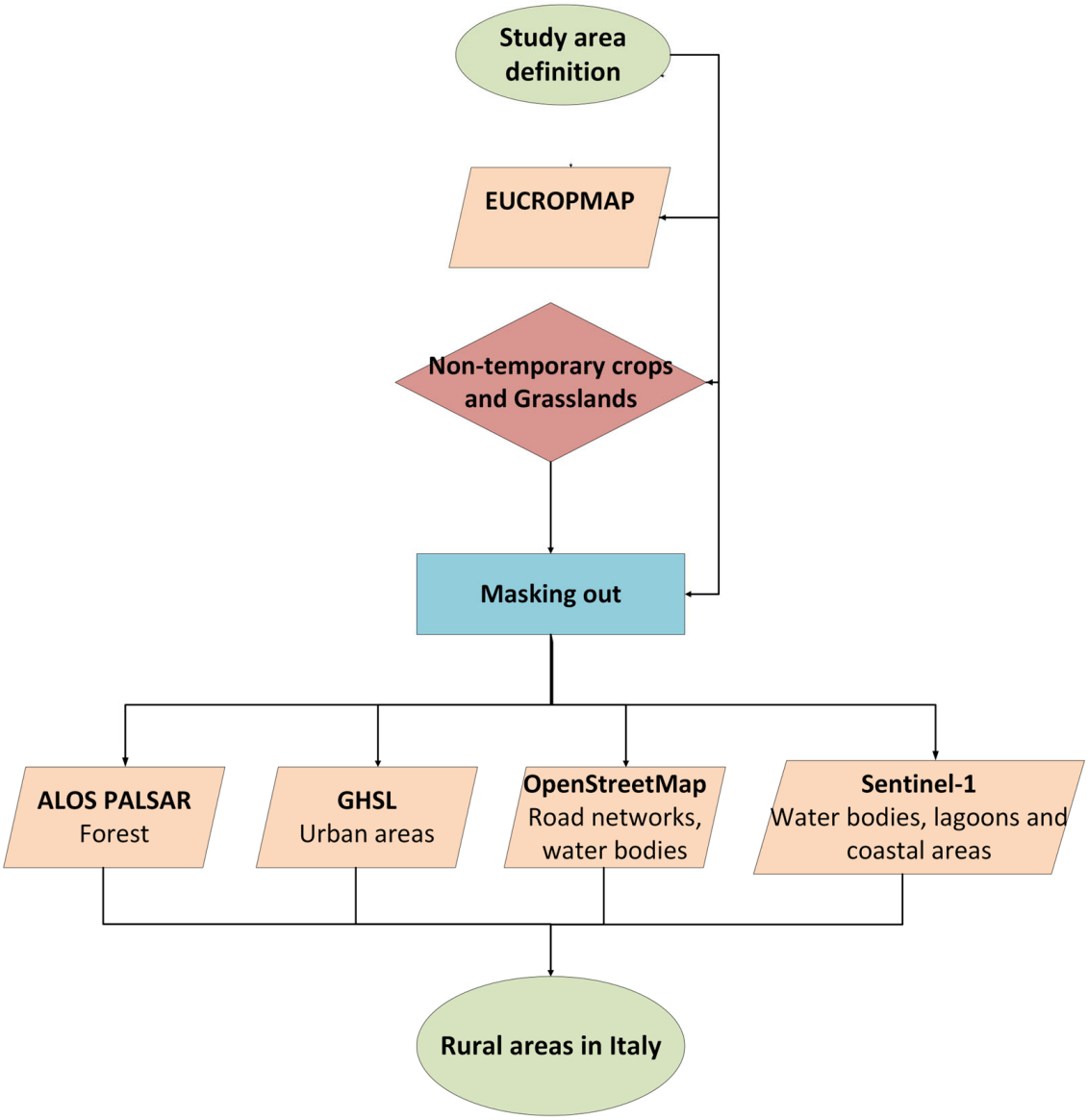

Figure 1. Flowchart for the identification of study areas.

Additionally, these models were chosen because they serve a specific time period and functional scope. MEDALUS pinpoints current degradation states, while LDN tracks the long-term trends of the study area. Both LDN and the Albedo–Vegetation model evaluate the delta between a baseline and a reference period. In terms of specific functions, MEDALUS and LDN have been employed to identify areas at risks, while the Albedo–Vegetation model has been used to monitor functions [9].

Based on the outcomes, strengths, and limitations of these existing models, the study proposes a new remote sensing model tailored to specifically monitor LD in rural areas that is scalable across different spatial contexts and replicable for future applications. Results from the MEDALUS, LDN SDG 15.3.1 and Albedo–Vegetation models are available in the Supplementary Materials (Figures S2, S4 and S6).

The image below (Figure 3) summarizes the approach adopted and described in detail in the following paragraphs.

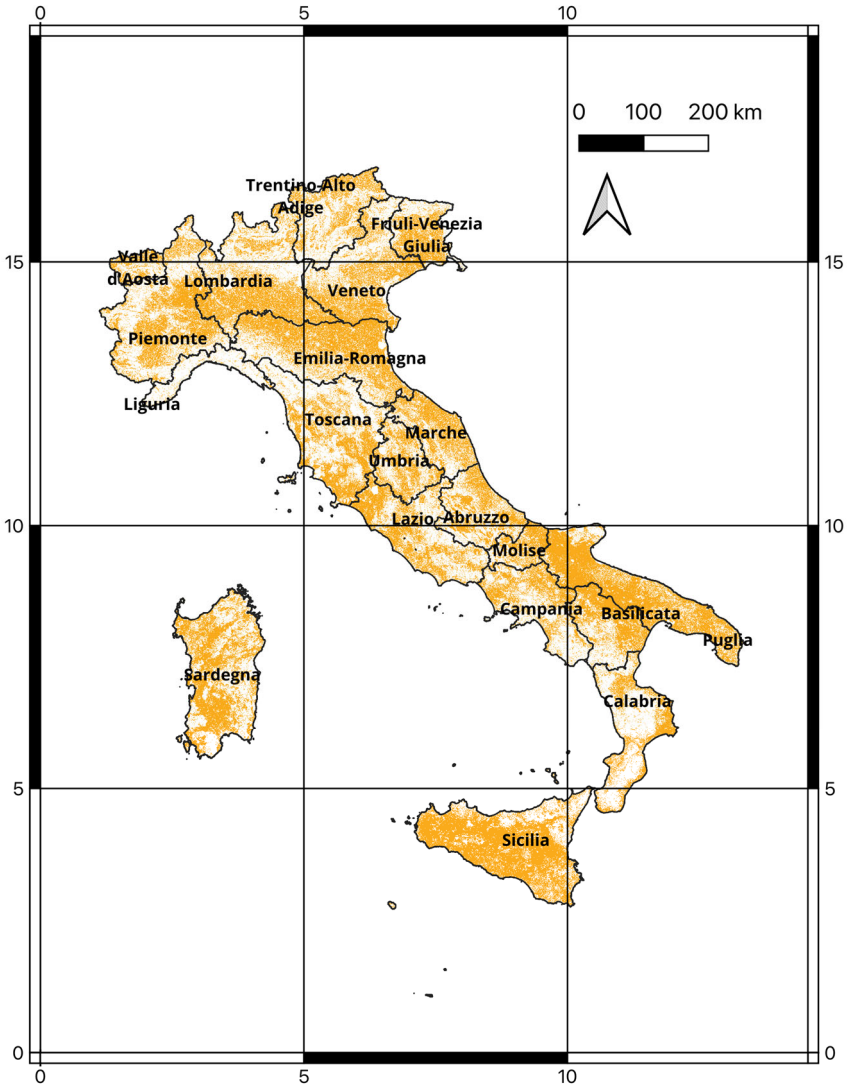

Figure 2. Study area: rural areas in Italy with regional administrative units.

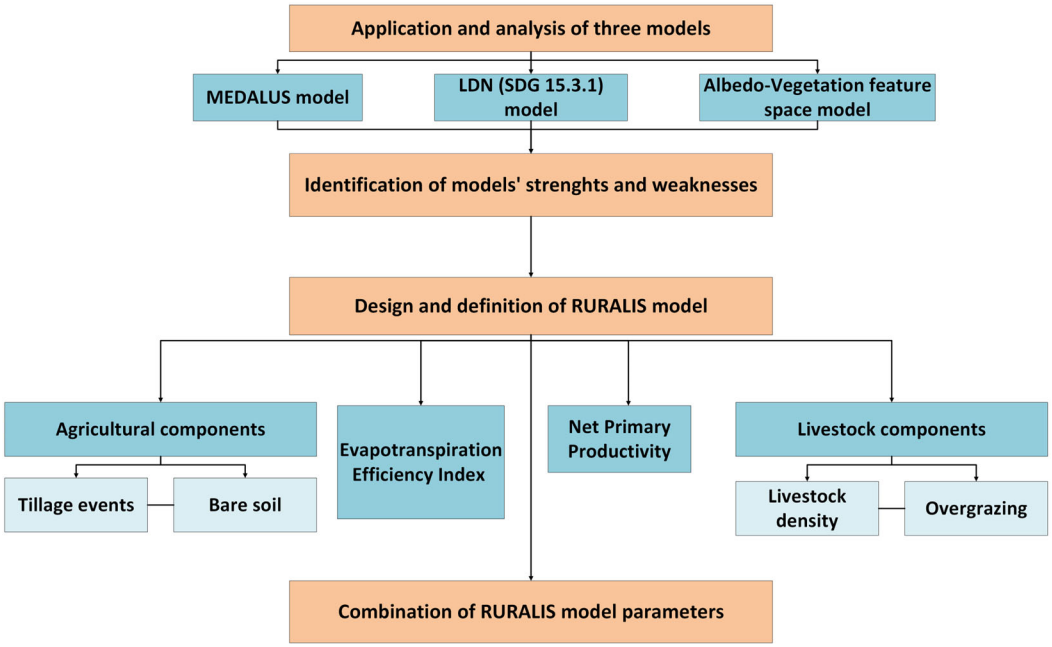

Figure 3. Flowchart of RURALIS model development.

Satellite images were downloaded with GEE using different geometries, employing a grid system of 4 big tiles for North, South, Centre and Islands or 121 small tiles covering the whole country, depending on data and resolution loads, to facilitate the computation process. The Global Administrative Unit Layers (GAUL) dataset was employed to retrieve the country administrative boundaries [49]. Additionally, optical images were also masked out from cloud cover. All images were converted to the EPSG 32633 Coordinate Reference System (CRS) and downloaded as GeoTIFF.

Once downloaded, satellite images were clipped on rural areas, combining Python (version 2.6.4) [50]—for computation and analysis—and QGIS—for visualization and map generation.

2.3. MEDALUS Model

Originally developed within the EU-funded project MEDALUS [20] to identify areas at risk of LD and desertification in the Mediterranean, the Environmentally Sensitive Area Index (ESAI) has since been applied at the global level [51]. The model integrates both a qualitative and quantitative approach [52], assessing environmental sensitivity based on four key factors: soil, climate, vegetation, and land use [53].

Each factor is represented by a specific quality index: Soil Quality Index (SQI); Climate Quality Index (CQI); Vegetation Quality Index (VQI); and Management Quality Index (MQI). Each indicator is calculated using multiple variables, which are classified into uniform classes. A sensitivity score is then assigned to each class to reflect its contribution to degradation [54].

The Soil Quality Index considers the following: the parent material, an important determinant of soil nutrients [55] extracted from the Lithological Map of Italy developed by the ISPRA (1:100 K) [56]; the slope grade, which represents a key component of soil surface and heavily influences soil properties [57], calculated from NASA SRTM Digital Elevation (30 m) [58]; and soil texture, drainage, and rock fragments, retrieved from the Harmonized World Soil Database v2.0 (HWSD) (1 km) [59], as they play a crucial role in assessing soil structure and fragility [60].

The Climate Quality Index captures paradigmatic aspects currently subjected to high variability and uncertainty, especially within the Mediterranean region [61]. The precipitation (mean value) from 1981 until 2023 was retrieved from Climate Hazards Group InfraRed Precipitation with Station (CHRIPS) [62]. The Aridity Index (AI), calculated as the ratio between monthly precipitation and the potential evapotranspiration (PET), where PET is estimated according to the Thornthwaite's method from monthly temperature [63], was retrieved from fifth generation of ECMWF atmospheric re-analyses of the global climate (ERA5) [64], with a final resolution of 5 km.

The European Space Agency (ESA) Climate Change Initiative (CCI) Global Land cover map v. 2.1.1 (300 m) [65] was instead employed for the Vegetation Quality Index, considering, for each land-cover category of the study area, the extent of vegetation protection to drought, fire, and erosion [20]. Additionally, plant cover was considered to evaluate the condition and health of the vegetation [66], calculating the average Normalized Difference Vegetation Index (NDVI) value for the period 2018–2024, extracted from Terra Moderate Resolution Imaging Spectroradiometer (MODIS) Vegetation Indices Monthly Version 6.1 (MOD13A3V6.1) [67] and resampled at 300 m.

Lastly, for the Management Quality Index, the ESA CCI Land cover map v. 2.1.1 was employed for land use intensity, while for population density, statistical data related to population and administrative boundaries related to 2024 were extrapolated from the Italian National Institute of Statistics (ISTAT), merged and projected at 300 m, to assess the anthropogenic pressures [68].

The related sensitiveness scores, ranging from 1, which indicates a low sensitivity to LD, to 2, which indicates a high sensitivity to degradation, were applied to each single variable and are reported in Table 1 [51]. The geometric mean of the scored variables was calculated to determine the value of the four quality indexes (SQI, CQI, VQI, MQI). Subsequently, the Environmentally Sensitive Area Index (ESAI) was derived by calculating the geometric mean of the quality indexes, using the same scoring scale [33], as exemplified in the formula below:

$$ESAI = (SQI \times CQI \times VQI \times MQI)^{1/4} \quad (1)$$

The spatial distribution of the sensitivity index was mapped for the area of interest [69].

Additionally, an environmental critical factor (ECF) index was calculated by counting, for each pixel, the number of variables with an ESA index score > 1.425, which corresponds to the C2 "critical" threshold, This allowed for a more comprehensive assessment of land degradation (LD) risk [51].

Table 1. Type of ESAs and corresponding ranges of the ESA index [51].

Land Type	Land Subtype	Sensitivity Ranges
Not affected	N	$\geq 1.00 \leq 1.170$
Potentially affected	P	$>1.170 \leq 1.225$
Fragile	F1	$>1.225 \leq 1.275$
	F2	$>1.275 \leq 1.325$
	F3	$>1.325 \leq 1.375$
Critical	C1	$>1.375 \leq 1.425$
	C2	$>1.425 \leq 1.530$
	C3	$>1.530 \leq 2.000$

2.4. LDN SDG 15.3.1 Model

In the context of the 2030 Agenda for Sustainable Development, 17 Sustainable Development Goals (SDGs) were adopted by the United Nations (UN) Member States to pledge the international community to the more sustainable management of the Earth's resources [70]. Among these, target 15.3 from SDG 15 "Life on Land" aims to achieve a land degradation-neutral world by 2030. To track progress toward this target, the indicator 15.3.1 was designed, which measures "the proportion of land that is degraded over total land area" as an indication of Land Degradation Neutrality (LDN). The indicator is based on changes over time between a baseline period and a reporting period of three sub-indicators: land cover, land productivity, and carbon stocks [40,71].

Land cover describes the physical cover of land surface, mapping different types of vegetation, water bodies and human infrastructure [72]. Within the SDG 15.3.1 framework, the land-cover role is twofold: first, it helps to detect degradation when there is a loss of ecosystem service productivity. Second, a land-cover classification system is crucial to disaggregate the other two sub-indicators according to existing and past land cover [73].

For assessing land-cover transition, the Global 30 m Land Cover Change (GLC_FCS30D) Dataset (30 m resolution) was used [74]. Its 36 land-cover categories were reclassified into the 6 UNCCD land-cover categories based on the Intergovernmental Panel on Climate Change (IPCC) classes: forest land; grassland; cropland; wetlands; settlements; and other land. Water bodies were added as a 7th category [75]. A transition matrix was then generated [76] for both the baseline period (2000–2015) and the reporting period (2015–2022), producing two transition maps that show changes in land cover during baseline and monitoring periods. The same time frame was also used for land productivity and carbon stocks.

Land productivity represents the rate of biomass accumulation, typically expressed as Net Primary Productivity (NPP)—the difference between gross primary productivity and plant respiration [77]. It is a key indicator of land health and productive capacity [78]. Annual productivity estimates were derived from three complementary metrics: trend, which measures long-term changes of land productivity; state, which reports temporal productivity as it compares current productivity against historical records in a given area; and performance, which reports spatial productivity, as it maps productivity among similar areas [76].

While NPP products derived from remote sensing are available, their resolution is still coarse [79]; therefore, the NDVI, as a proxy of NPP, was employed [80]. This is simpler to use than NPP and is of value with respect to adding information on variability; it was derived from 30 m Landsat 5 [81] and Landsat 7 [82] collections for the baseline period, and Landsat 8 [83] for the monitoring period. Additionally, to minimize the influence of climate variability and isolate anthropogenic factors, a climatic calibration was performed using the Rainfall Use Efficiency (RUE)—the ratio of annual NPP to annual precipitation—sourced from CHRIPS (~5 km resolution) [62]. This adjustment was integrated to account for precipitation variability on productivity trends, which is especially recommended for water-limited regions like southern Italy [84,85].

The three metrics (trend, state, performance) were then combined into a single productivity sub-indicator, where areas were classified as degraded, stable, or not degraded [77]; a productivity map was issued at a 30 m resolution.

The carbon stock quantifies the reserve that can accumulate or emit carbon; it is composed of above and below-ground biomass, dead organic matter and soil organic matter [86]. It is measured by the Soil Organic Carbon (SOC) stock, which reports information on the overall soil quality and the balance between organic matter gains and losses [73].The OpenLandMap Soil Organic Carbon content, at a 30 cm depth, was employed (250 m resolution) [87]. Carbon stock changes were calculated according to the Tier 1 approach defined by IPCC [86], applying conversion coefficients for changes in land use and a change factor associated with land use (FLU) [88,89] tailored for the Italian climatic zone [90]. Both the direction of change and the magnitude of the relative percentage change in SOC stocks, relative to a defined threshold, between the baseline and reporting period, was assessed [76]. The final SOC stock change maps were resampled at a 30 m resolution for consistency.

Once these were computed—all three sub-indicators and maps—the statistical principle of "One Out, All Out" (1OAO) was applied. According to this, if any one sub-indicator for a land unit is classified as negative (or stable if the area was already degraded in the baseline), then the unit is considered degraded.

Lastly, considering when degradation has occurred, a degradation type map with three classes—persistent, recent and improving—was issued for the different land-cover classes [40,76].

2.5. Albedo–Vegetation Feature Space Model

This approach applies a degradation difference model based on the Albedo–Vegetation feature space [91].

Albedo is a physical parameter representing the extent of energy absorbed by the underlying surface and the reflection characteristics of the surface to solar shortwave radiation [92], making it sensitive to different soil surface conditions such as soil moisture, vegetation cover, and snow [12]. In areas experiencing high temperatures and reduced precipitation, which often lead to a decline in vegetation and surface moisture, albedo tends

to increase [93]. This inverse relationship with vegetation makes albedo a useful indicator of LD and desertification processes.

To explore this relationship, three vegetation indexes were calculated and compared against Albedo: NDVI; the Modified Soil Adjusted Vegetation Index (MSAVI); and the Radar Vegetation Index (RVI).

NDVI is biophysical parameter reflecting the condition of surface vegetation, employed to monitor vegetation growth status and vegetation coverage [92]. While it performs well in areas with dense vegetation where soil influence is minimal [94], in sparsely vegetated areas, NDVI can be affected by soil background noise [12]. To overcome this limitation, the Soil Adjusted Vegetation Index (SAVI) introduced a constant soil adjustment factor (L) that minimizes soil influences on canopy spectra, improving vegetation estimates, especially in bare lands. However, since L is fixed, it does not adapt to varying vegetation densities. For this reason, the MSAVI replaces the constant L with a variable one, making it more responsive to vegetation-cover changes [95]. MSAVI can be efficiently utilized to assess the status of vegetative cover, especially in arid or semi-arid regions where vegetation is sparse and noise from non-vegetated surfaces needs to be minimized [96]. Compared to the above-mentioned optical vegetation indexes, RVI has the advantage of not being affected by cloudiness and lighting, allowing for the vegetation monitoring of crop growth during all seasons. Furthermore, it shows sensitivity to biomass and vegetation water content, and is poorly affected by environmental external conditions [97,98].

For this analysis, all vegetation indexes were calculated and downloaded from Sentinel-1 and Sentinel-2 (10 m), taking one image for the baseline year (2018) and another one for the change reference year (2024). The images refer to the summer period (June–September) to capture the peak of vegetative growth in crops with different phenological cycles [99] and to avoid confusion between seasonal bare soil and degradation signals [100]. Albedo was instead retrieved from Landsat 8 (30 m) for the same reference periods and atmospherically corrected.

To compare albedo and NDVI, MSAVI, and RVI, the latter were resampled at 30 m of resolution, and both albedo and the vegetation indexes were normalized and gridded into 32 tiles. By extrapolating 1 point of every 1000 valid pixels for each geographic area, a climate classification was applied considering the total annual precipitation and average annual temperature. Annual precipitation was downloaded from CHRIPS (~5 km resolution) [62], while daily average temperatures were retrieved from NASA NEX-GDDP (~25 km resolution) [101], for both 2018 and 2024.

Based on this, three climate classes were defined: "Cold and humid weather", characterized by high levels of precipitation (>600 mm/year) and rigid temperatures (<15°); "Intermediate weather", with moderate precipitation (300–600 mm/year) and temperatures (<20°); and "Arid and hot weather", presenting scarce precipitation (<300 mm/year) and hot temperatures (>20°).

A linear regression was then performed between each vegetation index and albedo (Albedo–NDVI; Albedo–MSAVI; Albedo–RVI) to model the linear relationship. Subsequently, a Degradation Difference Index (DDI) was calculated for 2018 and 2024, measuring, for each pixel, the difference between the observed and the expected values of albedo and NDVI, MSAVI, or RVI. This difference represents a measure of the degree of degradation against the expected condition.

To refine the analysis, negative values representing snow, water bodies, cover, forest, urban areas, roads were further masked out [96,102–104].

Lastly, DDI values were classified into 5 classes: Marked restoration between −6.0 and −4.5; Slight restoration between −4.5 and −3.0; No change between −3.0 and −1.0; Slight degradation between −1.0 and 0.0; and Marked degradation between 0.0 and 1.0 [92].

2.6. Limits and Advantages of the Analyzed Models

The main purpose of this article is to develop a model capable of capturing the specific environmental conditions of rural areas in Italy. To achieve this, a "model-learning" approach was adopted, inspired by the principles of reverse engineering. This method allowed for the extraction of insights and lessons from existing LD models by analyzing their structure, functionality, and applicability through direct implementation in the reference area [105].

Among the assessed models, the MEDALUS framework stands out for its adaptability. Originally conceived as a flexible framework [51], MEDALUS can be customized based on data availability and the characteristics of the study area. Several studies have expanded this model by including additional factors and their interactions [106–108], highlighting its potential for innovation [33]. Basso et al. [38] also noted that ESAI classes do not represent fixed values of environmental sensitivity. Instead, they are based on relative scores that measure sensitiveness within a specific area, while the final sensitivity classification provides a common framework for comparing the environmental sensitivity of various parts of the study area. This makes MEDALUS suitable for assessing several types of degradation or desertification, especially at a large scale or national scale [109].

Despite these strengths, MEDALUS presents limitations when considered for continuous monitoring. Some layers, such as soil type, are static, and the model accuracy depends heavily on the quality and resolution of input data. Additionally, the heterogeneity in spatial resolution among data sources can result in resolution inconsistencies, particularly in this model, which integrates datasets ranging from the 27.8 km resolution of the ERA5 database (used for evapotranspiration) to the 30 m resolution of the Digital Elevation Model (DEM), requiring further efforts for data harmonization and resampling. Moreover, adapting the framework to diverse datasets introduces challenges in reclassification and conversion to MEDALUS-compatible classes, necessitating knowledge of both of the study area and expertise on the influence of the specific parameter on LD [108]. The absence of temporal dynamics in the model is another critical limitation, particularly as climate variability and land use change play key roles in degradation processes [110].

The LDN SDG 15.3.1 indicator, endorsed for national reporting [39], relies on three sub-indicators to monitor ecosystem service provision. It is supported by a simple computation method (1OAO) [40,76] and various tools such as Trends. Earth [88] or System for Earth Observation Data Access, Processing and Analysis for Land Monitoring (SEPAL) [111], which facilitate data access and processing. However, this approach does not quantify the degree of degradation, only its temporal classification (e.g., recent or persistent) [40]. Additionally, the limited scope—relying solely on three sub-indicators—can result in misclassifications if not validated and contextualized appropriately [112].

The reliability of sub-indicators is also constrained by technical issues. With respect to land-cover classification, while remote sensing is improving its capacity to monitor land cover, it still remains affected by the limited availability of historical high-resolution time series and the simplistic representation of complex land transformations, especially when, as in this case, some classes are excluded from the analysis [113].

Land productivity was assessed using NDVI, as recommended by [76], to preserve spatial resolution. However, NDVI remains a proxy for NPP and may not fully capture seasonal variability, limiting its accuracy [85,114].

SOC changes may represent the biggest limitation of the application of this model at the national level. Unless there is a chance to gain access to more accurate data, current global SOC datasets (e.g., SoilGrids, OpenLandMap) used for Tier 1 assessments provide static data, making dynamic analysis challenging [115] and often reducing practical implementation to a two-sub-indicator system [76].

Another limit of the SDG model and its definition of a baseline period, is the representativeness of the selected baseline period, which might be influenced by specific land management and climatic conditions [76].

The Albedo–Vegetation model similarly suffers from limitations linked to time series availability. Without time series, its results reflect only snapshot conditions, making it difficult to distinguish real trends from seasonal or interannual fluctuations [33]. Additionally, the use of multiple vegetation indices confirmed that MSAVI is more sensitive in areas with sparse vegetation, while NDVI performs better in areas with dense vegetation. This variation makes it challenging to capture both rotational and permanent crops—characteristic of different zones within the study area—using a single index [12,96].

Another limitation is that scaling this model to a national level is computationally intensive due to the high resolution of Sentinel imagery. To manage this, the 32-tile grid was employed, with random points sampled from each tile. This method has preserved spatial heterogeneity and included underexplored regions, despite limiting local knowledge-based validation.

Nevertheless, the Albedo–Vegetation model represents an easy, powerful, simple, quick, and efficient method to monitor degradation, which can be implemented using different satellites and sensors and at different scales [116], and is preferable to extracting information solely from land-cover classification [117].

2.7. RURALIS Model

The RURal Areas Land Degradation Indicator System (RURALIS) model was specifically developed for the target area—rural regions—by incorporating key parameters that reflect the main drivers and indicators of LD. Evapotranspiration evaluates the capacity of the soil and vegetation to absorb and retain water. Bare soil occurrence and tillage frequency were used to assess the impact of intensive and unsustainable agricultural practices on soil health. The effects of unsustainable livestock management were also considered, as this factor, together with bare soil and tillage, provides insight into the anthropogenic pressures contributing to LD in the agro-pastoral landscapes of rural lands. Lastly, to assess vegetation degradation, land productivity was employed as an indicator.

The following paragraphs describe, in detail, how each of these parameters was calculated.

2.7.1. Evapotranspiration

Evapotranspiration (ET) is the combination of two processes, evaporation and transpiration, in which water is turned into vapor and then removed from the surfaces. These surfaces are, respectively, the soil surface and the crop. ET depends on: climate parameters (solar radiation, air temperature, air humidity, wind speed); crop factors (crop type, variety, development stage etc.); and management and environmental conditions (soil salinity, fertility, soil water content, cultivation practices etc.) [118].

The model has developed an Evapotranspiration Efficiency Index (EEI), derived from the ratio between actual evapotranspiration (ETa) and potential evapotranspiration (ETp) [118,119], as follows:

$$EEI = ETa/ETp \quad (2)$$

ETp was calculated according to the FAO Penmann–Monteith method, considering the sum of net solar radiation and net thermal radiation to derive net radiation, using ERA5-Land data [120]. ETa was calculated employing the Two Source Energy Balance (TSEB) model [121], based on the research of Guzinski et al. [122] and adapted from the SEN-ET Sentinel Application Platform (SNAP) plugin [123] with the following adjustments. First, the crop type maps developed by the Joint Research Centre (JRC) [42,124] were employed rather than a land-cover map. For each crop type, a crop coefficient (Kc) that represents the

effect of crop type and growth stage was retrieved from [118]. Second, for the biophysical parameters, NDVI was employed not only for its linear relation with Kc [125,126], but also for its simplicity, despite this potentially leading to limitations in sparsely vegetated areas. Moreover, based on the linear relation between NDVI and Kc [127], a linear interpolation was performed to estimate a dynamic Kc (Kc dyn) and capture the effect of the growth stage across the study area.

Another difference from Guzinski et al. [122] is that only the Leaf Area Index (LAI), leaf coverage (FCOVER) and the fraction of absorbed photosynthetically active radiation (FAPAR) were employed; these were obtained from the SNAP Biophysical Processor [128].

The Land Surface Temperature (LST) was calculated through Landsat 8 rather than Sentinel-3 to maintain a high level of resolution, while net solar radiation and net thermal radiation, in order to derive net radiation and climate parameters (temperature, wind speed, atmospheric pressure), were calculated using ERA5-Land rather than ERA5 to ensure a higher level of resolution and preserve the advantage of its bands.

Furthermore, the two parts of Eta, for both soil and crops, were modulated by introducing a soil factor to effectively reflect the available water (expressed as $(Mo - \theta_{WP})/(\theta_{FC} - \theta_{WP})$ where Mo is the soil moisture, θ_{WP} is the soil water content at wilting point, and θ_{FC} is the soil water content at field capacity [118]) and Kc to reflect crop characteristics.

The table below (Table 2) describes the input parameters and sources used for the ETp and ETa calculations.

Table 2. Input sources and parameters for ETp and ETa calculations.

Index	Parameter	Source/Reference	Resolution	Periods
ETp	Temperature Wind speed Atmospheric pressure Net solar radiation Net thermal radiation	ERA5-Land monthly averaged data [129]	~11 km	2017–2024
ETa	Crop type	EUCROPMAP 2018 [42] EUCROPMAP 2022 [124]	10 m	2017–2021 2022–2024
	NDVI LAI Albedo	Harmonized Sentinel-2 MultiSpectral Instrument (MSI) [45]	10 m 10 m 20 m	2017–2014
	DEM	NASA SRTM Digital Elevation [58]	30 m	NA
	Soil texture	SoilGrids [130]	250 m	NA
	LST	Landsat 8 [83]	30 m	2017–2024
	Soil moisture	NASA SMAP [131]	9 km	2017–2024
	Temperature Wind speed Atmospheric pressure Net solar radiation Net thermal radiation	ERA5-Land monthly averaged data [129]	~11 km	2017–2024

ETp was resampled at a 20 m resolution to match with the ETa resolution, and the EEI was calculated. It measures how efficiently the soil and crops use available water. A high EEI value (close to 1 or >1) indicates a favorable water condition with the soil and crop in good status, while a low value (<1) indicates water stress or soil or crop degradation. Annual EEI maps were developed from 2017 to 2024.

2.7.2. Bare Soil and Tillage Exposure

Bare soil, defined as areas with low or no vegetation cover, has been recognized as a key driver of LD. Due to the absence of organic matter and the stabilizing effect of plant roots, bare soil is more prone to erosion [132–134] and contributes to reduced water retention and increased surface runoff [135]. Similarly, the implementation of over-deep tillage practices (above 35 cm depth) can accelerate LD [132], as these practices disturb the soil structure, leading to soil erosion [136], and reduce the soil's capacity to retain water and nutrients. Furthermore, over-deep tillage may stimulate the mineralization of SOC [137], which in turn leads to SOC decomposition and the release of CO_2 into the atmosphere [138]. When combined, bare soil and over-deep tillage can significantly compromise soil quality [139].

To map the frequency of bare soil, all Sentinel-2 images from each year within the reference period (2017–2024) were processed to calculate NDVI. A binary classification was applied, identifying bare soil as pixels with NDVI values below 0.20 [140]. A mask for agricultural areas was applied using the crop classes from EUCROPMAP; the number of bare soil events per pixel per year was computed.

For mapping over-deep tillage, a combined approach using Sentinel-2 and Sentinel-1 data was adopted. First, the same NDVI-based binary classification was applied to Sentinel-2 imagery, this time using a slightly higher NDVI threshold (0.30) to also include sparsely vegetated areas. Instead of calculating event frequency, only pixels identified as bare at least once before the Sentinel-1 passage were retained. Again, the EUCROPMAP-based crop mask was used to isolate agricultural areas. Sentinel-1 VV radar images were then employed to detect tillage events over the bare soil pixels. For each location, two images from the same orbit were selected; over-deep tillage was identified by calculating the backscatter difference, considering a threshold of >2 dB to flag tillage activity [141]. Lastly, the number of tillage events was recorded for each pixel and for each year.

2.7.3. Livestock Impact

Livestock production substantially affects various environmental resources, including soil and water, and requires targeted attention and intervention in both intensive and extensive farming systems to mitigate these impacts [142]. Overgrazing is widely considered one of the most significant drivers of soil degradation, particularly in Mediterranean regions. Its impact is often intensified when combined with other anthropogenic pressures, leading to both direct and indirect effects. Directly, overgrazing causes soil compaction, which reduces soil porosity and inhibits water infiltration, ultimately increasing surface runoff. Indirectly, it contributes to vegetation loss and to a decline in plant biodiversity, which can result in soil crusting and soil organic matter reduction [143].

Another problem associated with livestock is manure application to agricultural fields. While the application of manure to agricultural fields has been shown to enhance soil fertility, repeated and excessive use can negatively affect the soil physical, chemical, and biological properties. This over-application increases the risk of nutrient loss through leaching, particularly nitrogen, which can contribute to nitrous oxide (N_2O) emissions—an important greenhouse gas [144].

To assess livestock pressure, two complementary approaches were combined: the CAIA model [145], which estimates the impact of grazing on soil, and the livestock density model employed by Gabriele and Previtali [146], which links livestock distribution to manure availability, and, consequently, to the risk of nutrient leaching from agricultural areas. For both models, an Extract, Load and Transform (ELT) data processing approach was applied, where data were first extracted from national databases, loaded into the spatial reference target system—pastures and agricultural zones in rural Italy—and then transformed to apply the two respective models.

For the CAIA model, the number of livestock animals under grazing was extracted for the reference period (2017–2024) from the National Livestock Registry, considering only cattle, goats and sheep under extensive farming system per municipality. Since cattle data were only available from 2018 onward, the 2017 value was estimated using the average from subsequent years. First, for the loading phase, pastureland was identified by extracting grassland areas (hectares) from EUCROPMAP using a binary classification. The grassland maps was intersected with the administrative boundaries, by municipality, retrieved from ISTAT [147]. This allowed for the number of livestock animals per municipality to spatially match pasture areas. In the transformation phase, average weights were assigned to each species based on studies in the literature (453 kg for cattle, 42 kg for sheep [148], and 52 kg for goats [145]), while species-specific weighting factors for productivity and extensive management were drawn from research by Pulina and Zucca. The lower the index, the lower the land productivity and the more prone the soil is to degradation [145].

For the livestock density model, the number of non-grazing livestock animals per municipality (cattle, goats, sheep, pigs, rabbits, Equidae and poultry) was extracted from the National Livestock Registry for the same reference period, applying also the same strategy for the missing data explained above. The spatial loading procedure is the same as that used in the CAIA model, with the only difference being the use of cropland areas from EUCROPMAP to define the Utilized Agricultural Area (UAA). In the transformation phase, each animal unit was converted to Livestock Units (LS) using the Eurostat Livestock Unit Coefficient Index [149]; livestock density was calculated as the ratio between the total livestock units and the UAA. The higher the livestock density, the greater the risk of nutrient leaching and soil degradation.

2.7.4. Land Productivity

As emphasized by the LDN model, land productivity is a key indicator of the land's capacity to support biomass growth; it reflects changes in ecosystem functioning over time. In this model, however, land productivity was assessed using NPP instead of the more commonly used NDVI. This decision stems from the fact that NDVI is not a direct measure of biomass production. Rather, NDVI reflects the proportion of solar radiation absorbed by chlorophyll in green vegetation, which is only indirectly related to NPP. In contrast, NPP provides a more accurate estimate of actual biomass accumulation, as it is generally positively correlated with plant biomass—more biomass implies more foliage engaged in photosynthesis, resulting in higher NPP values [73].

As the only available dataset with annual updates is the MODIS MOD17A3HGF V6.1 product [150], this was downloaded from GEE for the reference period (2017–2024).

2.7.5. Parameters Integration and Degradation Index Development

For each parameter, annual average values were computed at the pixel level. Based on these yearly values, four dynamic thresholds were derived from quintiles (20%, 40%, 60%, 80%) to classify the parameter ranges. These thresholds were then used to categorize the parameter values, the temporal trends, into five discrete classes ranging from 0 to 4. All the resulting maps were then resampled to a common spatial resolution of 20 m.

To integrate the parameters into a single degradation index, multiple steps were followed. First, the Analytical Hierarchical Process (AHP) was applied to assign weights to each parameter based on their relative importance in contributing to LD, granting that each parameter's impact was well represented. The Consistency Ratio (CR) was calculated to validate the consistency of the pairwise comparisons, accepting only results with a CR $\leq$ 0.10 [151] across all rural areas, using a 32 tile grid. This allowed for the weight optimization to also reflect sub-regional contexts.

Next, the Weighted Linear Combination (WLC) was used to combine the different parameters. These were normalized and multiplied by their respective weights, resulting in a continuous LD index ranging from 0 to 1, where higher values indicate severe degradation [152].

To assess the robustness of the model, a Monte Carlo analysis with 50 iterations per tile was performed [153]. Lastly, a K-means clustering was applied to classify the index into four distinct LD classes from 1 (no degradation) to 4 (severe degradation) [154]. The table below (Table 3) reports the average weight assigned for each indicator. Details of the weights assigned to each indicator across the 32 sub-regional tiles are provided in the Supplementary Materials (Table S1 and Figure S1).

Table 3. Average indicator weights assigned across the 32 sub-regional tiles.

RURALIS Indicators	Average Weights
EEI	1.75
Bare soil frequency	22.61
Tillage exposure	22.49
Overgrazing	22.80
Livestock density	18.01
Land productivity	12.32

3. Results

RURALIS Model Results

Results (Figure 4) from the model show that more than 50% of Italy's rural areas—approximately 8,842,843.96 ha—fall under class RD (At risk of degradation). This is followed by around 5,000,000 ha (roughly 30%) classified as LD class (Light degradation). Less than 10% of rural land is categorized as either SD class (Severe degradation) or ND class (No degradation).

In terms of geographic distribution at the regional level (Figure 5), degraded rural areas (class LD and 4) are concentrated in Molise (56%), Veneto (54%), Emilia-Romagna (50%), Puglia (49.5%), and Sicilia (47%) collectively covering 3,117,475.44 ha. Other regions also show substantial degraded areas, ranging from Marche, with 647,127.04 ha (45%) to Sardegna, with 363,371.48 ha (27%). The least affected regions are Trentino-Alto Adige, and Liguria, where degradation affects only about 11% of rural land. Valle d'Aosta reports the lowest percentage of degraded rural area, with just 6463.24 ha (3.5%).

Focusing on SD class, Puglia leads, with 18% of affected rural areas (277,027.12 ha), followed by Molise (17%) with 277,464.68 ha, Veneto (16%) with 166,925.20 ha, Basilicata (15%) with 96,327.16 ha, and Emilia-Romagna (14%) with 201,862.04 ha.

For the LD class, degradation is more evenly distributed across the country. Molise, Veneto, Sicilia and Emilia-Romagna were shown to have more than 35% of their rural areas under the LD condition (around 1,800,000 ha) and all other regions show more than 20% of their rural lands in the LD class, except for Valle d'Aosta, Trentino-Alto Adige and Liguria, where less than 12% of the lands present with early signs of degradation. Nevertheless, these same regions also have the highest portion of lands at risk (RD class). Lombardia and Valle d'Aosta have also the highest share of rural areas not affected by degradation (28 and 26%, respectively), followed by Emilia-Romagna (203,998.08 ha; 14%) and Veneto (128,554.92 ha; 12%).

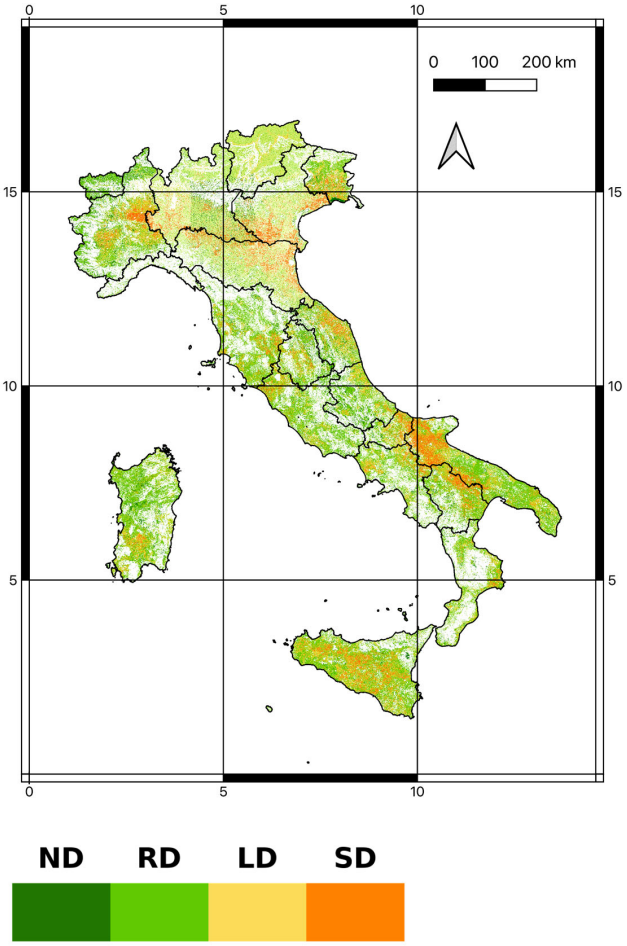

Figure 4. RURALIS model classification, where ND = no degradation; RD = at risk of degradation; LD = light degradation; SD = severe degradation (20 m resolution).

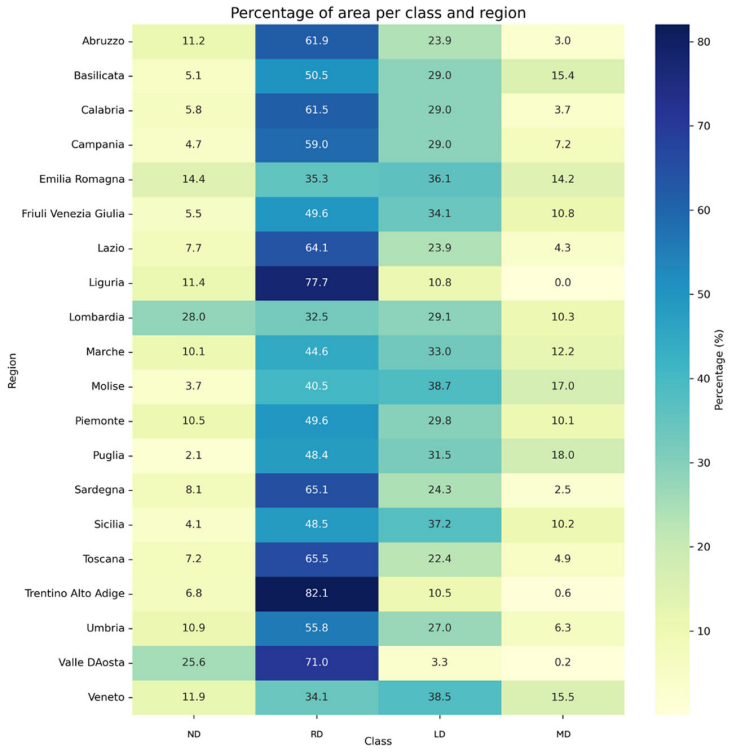

Figure 5. RURALIS model—percentage of area per class and region—heatmap.

4. Discussion

4.1. Design and Features of RURALIS Model

Based on these results, the RURALIS model was designed and developed by incorporating the strengths and addressing the limitations of the three reviewed approaches.

Table 4 summarizes and compares the indicator system, quantification methods, and data sources of the four models.

Table 4. Overview of indicator systems, quantification methods, data sources, and multitemporal approach for the four land degradation assessment models.

Model	Indicator System	Quantification Method	Data Sources	Multitemporal Approach
MEDALUS	- Soil Quality Index, - Climate Quality Index, - Vegetation Quality Index, - Management Quality Index	Geometric mean of the weighted quality indexes	- ISPRA Lithologic map (1 km) - NASA SRTM Digital Elevation (30 m) - Harmonized World Soil Database v2.0 (1 km) - Climate Hazards Group InfraRed Precipitation with Station (CHRIPS) (5 km) - ERA5 (27.8 km) - ESA Climate Change Initiative (CCI) Global Land cover map v. 2.1.1 (300 m) - Terra Moderate Resolution Imaging Spectroradiometer (MODIS) Vegetation Indices Monthly Version 6.1 (1 km) - ISTAT data on population density	Static (latest available dataset)
LDN SDG 15.3.1	- Land-cover change, - Land Productivity, - Soil Organic Carbon	One Out, All Out (1OAO) principle	- Global 30 m Land Cover Change 2000–2022 (30 m) - Landsat (30 m) - OpenLandMap Soil organic Carbon content at 30 cm depth (250 m)	Baseline period: 2000–2015 Monitoring period: 2015–2022
Albedo–Vegetation feature space	- Albedo - NDVI/MSAVI/RVI	Feature space classification	- Landsat (30 m) - Sentinel 1 and Sentinel 2 (10 m)	Baseline period: 2018 Monitoring period: 2024
RURALIS	- Evapotranspiration Efficiency Index, - Bare soil exposure, - Tillage frequency, - Livestock pressure, - Land Productivity	Composite index with context-specific weighting	- ERA5-Land (~11 km) - EUCROPMAP 2018, 2022 (10 m) - NASA SRTM Digital Elevation (30 m) - SoilGrids (250 m) - Landsat 8 (30 m) - NASA SMAP (9 km) - Sentinel 1 and Sentinel 2 (10 m) - Terra Net Primary Production Gap-Filled Yearly Global (500 m)	Period: 2017–2024

Regarding the temporal dimension, neither the MEDALUS nor the Albedo–Vegetation model prescribe a fixed observation period. Applications of MEDALUS range from short-term analyses, such as the two-year study by Ren et al. [109], to long-term investigations extending up to fifty years, such as in the work of Salvati et al. [155]. The Albedo–Vegetation model typically spans an average of 16.5 years, aligning closely with the UNCCD-recommended 15-year reference period. Beyond the baseline-period issue, the commonly adopted temporal window is largely derived from hydrological studies [156] and may not be optimal for all cases. Therefore, when SDG-based results in Italy show a tendency toward stabilization over time, this could be attributed to these two aspects. On the other hand, the Albedo–Vegetation outcomes suggest that shorter time windows may fail to capture meaningful variability. To reconcile the need for detail with the availability

of robust data, RURALIS adopts a medium-term analysis period (eight years or more), taking advantage of the increased data density provided by the launch of Sentinel-2B in 2017.

In terms of spatial resolution, RURALIS prioritizes the use of native high-resolution input layers, typically at 10 to 20 m, drawing from the strengths of the Albedo–Vegetation model. The only exception is NPP, which remains available only at coarser resolutions. This choice maximizes spatial accuracy and avoids the pitfalls associated with the resampling required by the SDG and MEDALUS models, where high-resolution outputs are often derived from coarser sub-indicators.

Although RURALIS is not structured as a formal framework, like MEDALUS, it follows a modular architecture that allows for integration and changes. This might be the case, for example, for missing data or parameters that may not be applicable to different contexts (e.g., livestock components). To accommodate local variability without compromising comparability, the model applies dynamic weight assignment.

The logic underpinning the model builds on is the class-weight structure of MEDALUS, with enhanced spatial granularity. The national territory is divided into 32 processing tiles, which facilitates computation and enables the model to maintain relevance at the sub-national level. Parameter weights are dynamically assigned through an integrated approach combining AHP, WLC and Monte Carlo simulations. This overcomes the rigidity of fixed scoring systems and ensures sensitivity to regional differences.

Additionally, in line with the recommendations by Ferrara et al. [51], RURALIS extends trend analysis to all parameters, rather than focusing solely on land productivity, as in LDN SDG 15.3.1. This comprehensive approach enables continuous monitoring and a better identification of degradation drivers over time.

The selection of input parameters was guided by the need to represent the key functional dynamics of rural landscapes, particularly those related to agriculture and livestock. To maintain this level of spatial detail, parameters and technologies were carefully selected, prioritizing high-resolution data and allowing for exceptions only when strictly necessary. In the case of NPP, rather than using NDVI as a proxy—as in the LDN approach—RURALIS directly incorporates NPP as a more meaningful indicator of land productivity. This decision is consistent with the rationale behind the Albedo–Vegetation model and is further supported by the limited representativeness of any single vegetation index in the Italian context, given their varying sensitivity to vegetation density and solar radiation. Indeed, findings from the Albedo–Vegetation model, which tested multiple vegetation indices, have underscored the ecological heterogeneity of the Italian landscape and the inadequacy of relying on a single index. This highlights the need for a data fusion approach, combining different parameters and technologies to better capture local variability. Furthermore, results from the Albedo–Vegetation model have also indicated the importance of designing a model suitable for both national and sub-national applications. For climate variables, although these were excluded as standalone layers due to their coarse spatial resolution, their influence was indirectly integrated through the computation of the Enhanced Environmental Index (EEI).

To better contextualize the proposed RURALIS approach, Table 5 summarizes the main similarities and differences in terms of indices and methodological frameworks when compared with the MEDALUS, LDN SDG 15.3.1, and the Albedo–Vegetation models.

Altogether, RURALIS offers a flexible, high-resolution, and updatable model structure for monitoring LD in rural contexts, capable of operating at both national and sub-national levels. By integrating temporal trend analysis and enabling modular adjustments, the model supports informed planning and monitoring of interventions for sustainable land management in rural contexts.

Table 5. Comparative analysis of similarities and differences among land degradation assessment models.

RURALIS	MEDALUS	LDN SDG 15.3.1	Albedo–Vegetation Feature Space
Evapotranspiration Efficiency Index (EEI) calculated according to the TSEB model as the ratio between actual and potential evapotranspiration. It is a composite index employing input data associated with climate, soil, crop type and orography.	Potential evapotranspiration calculated according to Thornthwaite's method from monthly temperature to derive the aridity index	Not employed	Not employed
Bare soil exposure	Not employed	Not employed	Not employed
Tillage frequency	Not employed	Not employed	Not employed
Livestock pressure	Not employed	Not employed	Not employed
Land Productivity calculated using the NPP product from MODIS	Not employed	Land Productivity calculated using the NDVI as proxy from Landsat	Not employed

Nevertheless, the model presents two main limitations. First, no validation was possible with ground data due both to the unavailability of suitable data and the incompatibility with available land degradation maps, for several reasons that are further detailed in Section 4.2. However, the model design does not exclude this option and further refinement with the integration of ground truth data and machine learning is recommended as it may improve the accuracy of weights appointment. Secondly, maintaining a high spatial resolution imposes considerable computational demand. This may be a barrier for users with limited access to processing infrastructure or those working at coarser scales.

While RURALIS does not aim to impose a standardized methodology for land degradation assessment, it demonstrates that context-specific approaches are essential for accurately capturing degradation dynamics, particularly in rural areas where agriculture and livestock interact intensively. In this regard, the framework offers both a methodological advancement—by integrating multiple remote sensing and modelling approaches in a flexible, modular structure—and a practical monitoring tool that can guide targeted interventions. At the same time, it is recognized that context-specific methods may increase the diversity of approaches, posing a trade-off between local adaptability and cross-study comparability.

4.2. Considerations on Model Validation

A quantitative validation of the RURALIS model could not be performed in this study due to several limitations. Ground-based assessments of severely degraded areas at the national scale are currently unavailable and the multidimensional nature of degradation processes makes it extremely difficult to build a reliable, spatially consistent ground dataset. This limitation is further amplified by the national extent of the present analysis. By contrast, in the case of soil degradation, European-level datasets could provide a validation baseline [157]; however, such datasets do not cover the broader concept of land degradation addressed in this article.

An alternative strategy would be to validate RURALIS against existing degradation maps. Two options were considered and analyzed: institutional maps and European maps. However, both approaches present significant methodological, tempo-

ral, and spatial inconsistencies that prevent their use for robust quantitative validation (see Sections 4.2.1 and 4.2.2).

As a more feasible approach, RURALIS was instead comparatively assessed against three well-established models (see Section 4.2.3), using a Random Forest analysis to evaluate the consistency of the degraded areas identified.

4.2.1. Comparative Analysis with Institutional Assessments of Land Degradation

When comparing the outputs of RURALIS with official assessments of land degradation conducted at the institutional level by the National System for Environmental Protection (SNPA) for validation, the task proves particularly challenging for several reasons. First, the scope of analysis differs substantially: while SNPA reports [39,158] and related studies [159] cover the entire national territory, this study has focused exclusively on rural areas. This inevitably leads to divergent results and helps to explain the discrepancies. For instance, Assennato et al. [159] reported that "degraded areas are concentrated mainly in fertile agricultural land and in correspondence of large urban areas", a dimension that RURALIS cannot capture, as urban areas were deliberately masked out. Similarly, both the SNPA reports (2021; 2024) emphasize that "land consumption directly or indirectly affects many of the degradation factors analysed", with land consumption itself defined as "a process associated with the loss of a fundamental, limited and non-renewable environmental resource, due to the occupation of an area that was originally agricultural, natural or semi-natural with artificial cover" [39,158]. Since RURALIS has excluded artificial land cover from its scope, this dimension could not be assessed. Temporal misalignment further complicates the comparison. RURALIS evaluates the period 2017–2024, whereas Assennato et al. [159] covers 2012–2018. The SNPA 2021 report refers to 2012–2020 [158] and the SNPA 2024 report [39] spans 2000–2019. Such inconsistencies in reference periods provide an additional source of divergence.

Lastly, discrepancies also stem from differences in input data, analytical factors, resolution, and methodologies. Beyond the methodological divergences already highlighted between the LDN SDG 15.3.1 framework—adopted by SNPA reports and Assennato et al.—and RURALIS, the two approaches emphasize different sub-indicators. RURALIS integrates context-specific data, such as evapotranspiration, livestock density, bare soil, and tillage exposure, whereas SNPA and Assennato et al., employ indicators more relevant to soil consumption analysis, as reported in Table 6. Consequently, the models also rely on different spatial resolutions: RURALIS prioritizes maintaining the highest possible native resolution by exploiting Sentinel data, while SNPA and Assennato et al., rely on Trends.Earth and coarser-resolution input datasets. While similar challenges arise when comparing the SNPA and Assennato et al. approaches with the MEDALUS and Albedo–Vegetation feature space, a qualitative comparison is more feasible with the LDN SDG 15.3.1 framework applied in this study. From a methodological standpoint, both the SNPA reports and the Assennato et al. study adopt a consistent approach; however, in terms of temporal coverage, the SNPA 2024 report aligns more closely with the time frame considered here. For this reason, the comparison presented below focuses specifically on the SNPA 2024 report and its outcomes.

From the methodology point of view, the table below (Table 6) synthetizes the main differences.

In terms of results, the SNPA 2024 report estimates that 21.4% of Italian territory is degraded, whereas the findings presented in this study indicate a degraded area of 11%. This discrepancy, which also appears to extend to the geographic distribution of degraded areas, may be partially explained by the exclusion of urban and forested areas in the present analysis. However, a more detailed quantitative comparison is not possible due to the unavailability of the underlying SNPA maps.

Table 6. Comparison between SNPA (2024) and LDN SDG 15.3.1 (present study).

Comparative Aspects		SNPA (2024) Report [39]	Present Study (LDN SDG 15.3.1)
Time frame	**Baseline**	2000–2015	2000–2015
	Reporting period	2004–2019	2015–2022
Study area		Italy	Rural areas in Italy
Input data	**Sub-indicator: Land-cover change**	Corine Land Cover 2000–2018 (100 m) SNPA soil consumption map (10 m)	Global 30 m Land Cover Change 2000–2022 (30 m)
	Sub-indicator: Land Productivity	NDVI calculated from MODIS (250 m) integrated with the calculation of Water Use Efficiency (WUE) from MODIS (500 m) as climatic calibration	NDVI calculated from Landsat (30 m) integrated with the calculation of RUE from CHRIPS (~5 km) as climatic calibration
	Sub-indicator: SOC change	Global Soil Organic Carbon Map at 0–30 cm (~1 km)	OpenLandMap Soil organic Carbon content at 30 cm depth (250 m)
Additional degradation factors		- Fragmentation - Area potentially affected by land consumption; - Areas with high and medium density of artificial cover; - Increase in unused spaces with an area of less than 1000 m^2; - Areas affected by fire in recent years.	Not available.
Processing tools		Trends.Earth GEE QGIS	GEE (version 2025) Python (version 2.6.4) QGIS (version 3.4.2.0)

4.2.2. Comparative Analysis with European Assessments of Land Degradation

The LMI developed by JRC [5] assesses land degradation in agricultural areas and, in principle, could provide a more comparable reference for validation than national institutional maps. However, substantial mismatches prevent a meaningful quantitative validation (Table 7). The most fundamental limitation lies in the conceptual approach: while the LMI defines LD as the co-occurrence of twelve distinct processes, RURALIS considers land degradation as a whole, focusing instead on the factors that contribute to it and can be monitored over time. Consequently, the RURALIS index expresses the degree of degradation, rather than the overlap of multiple processes.

Additional incompatibilities further hinder validation. Regarding the study area, both JRC and RURALIS focus on agricultural lands (arable land, permanent crops, pastures, and related areas). However, the basemaps differ: JRC relies on CORINE Land Cover (CLC, 100 m resolution), while RURALIS uses EUCROPMAP and ancillary datasets (10 m resolution), leading to inconsistencies in both spatial resolution and land-cover classification.

With respect to temporal coverage and resolution, JRC input datasets span between 1981–2021 and yield final outputs at the 500 m resolution, whereas RURALIS covers the period 2017–2024 with outputs at 20 m.

Table 7. Comparison between European assessment (LMI) and RURALIS.

Comparative Aspects	LMI [5]	RURALIS
Time reference	1981–2021	2017–2024
Study area	Agricultural areas in Europe, including Italy	Rural areas in Italy
Basemap	CORINE Land Cover 2018 (100 m)	EUCROPMAP 2018 (10 m)
Output resolution	500 m	20 m
Conceptual approach	LD as the convergence pattern of 12 LD patterns	LD as a whole complex pattern
Index	LMI highlights the number of interacting processes	RURALIS expresses the degree of degradation based on contributing factors
Methodology	No weighting system. Equal importance assigned to all degradation processes	Weighting system applied to all factors, considering spatial variability at a sub-national scale.

Lastly, in terms of methodology, the JRC approach, without adopting a weighting system, it assigns equal importance to all degradation processes, although in practice, their contributions may differ. In contrast, RURALIS applies a weighting system to factors, an approach widely adopted in the literature for its simplicity, and which, by the way it is designed, also addresses spatial variability at sub-national scale.

4.2.3. Comparative Analysis on Degraded Areas Among the Different Models

Given the diversity of the models examined in this study—and their inherent incomparability due to differing assumptions, timeframes, scales, land-cover maps classifications, resolutions, and outputs—a direct correlation among them is not feasible. To synthesize and compare their outputs more robustly, a Random Forest (RF) classification model was employed. This approach allows for the integration of heterogeneous model results and the generation of a coherent output map, which highlights areas that have been recognized as severely degraded by all four models.

The choice of the RF model over simpler rule-based classification methods (e.g., fixed thresholds or index voting) was motivated by, as follows: its ability to not rely on arbitrary thresholds, but to learn automatically from input data; capture non-linear and complex relationships between variables (such as interactions between NDVI, RVI, and MSAVI in specific territorial conditions); better generalize in the presence of environmental variability and noise in the data; provide reliable validation metrics such as accuracy, precision, recall and F1-score; and easily integrate the geospatial workflow, making it suitable for the production of consistent thematic maps.

The RF model was configured with 100 decision trees; reproducibility was ensured by setting a fixed random seed (random state = 42). The training dataset was obtained via random sampling, selecting up to 5 million valid pixels. These pixels were filtered using a common mask that excluded any with missing (no data) values across all input layers. Only the most severe degradation classes were retained for analysis: C1, C2, and C3 from MEDALUS; Degradation Class from the LDN SDG 15.3.1 framework; and the Marked Degradation Class and Severe Degradation Class, respectively, from the Albedo–Vegetation model and the RURALIS model.

The dataset was split into training (70%) and test (30%) sets using a stratified train-test split, ensuring a balanced distribution between "degraded" and "non-degraded" classes.

Model performance was evaluated on a test set of 600,000 pixels, achieving high accuracy and reliable class discrimination, with an overall accuracy of 0.89, precision of 0.89, recall of 0.92, and F1-score of 0.91. These metrics confirm that the model effectively distinguishes degraded from non-degraded areas within the analyzed data domain.

Based on RF results (Figure 6), around 2,344,791.64 ha of rural land in Italy—equivalent to 13.6% of the total rural area—have been identified as severely degraded, according to all models. At the regional scale, the northern part of Puglia shows the highest concentration of degraded areas, consistently identified across all models, followed by Sicilia. In contrast, degradation in northern Italy appears more spatially homogeneous, particularly affecting Emilia-Romagna, Lombardia, and Veneto.

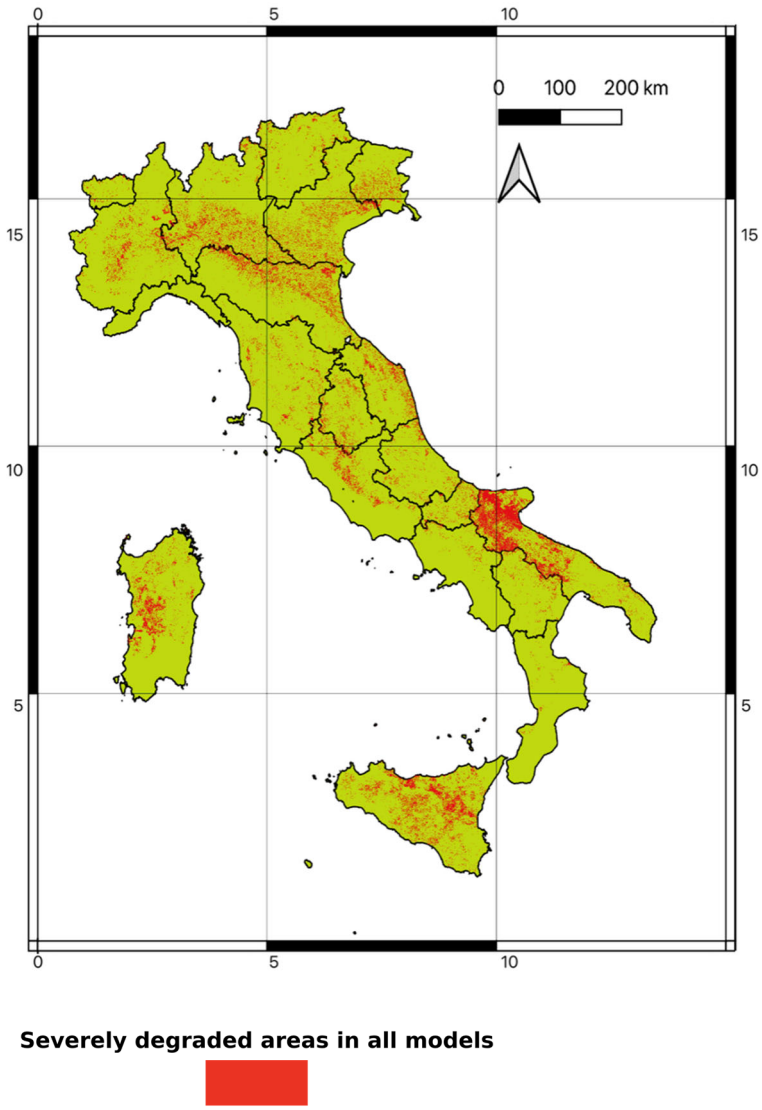

Figure 6. Severely degraded areas according to all models derived from RF.

Temporal trends derived from the RURALIS model help to contextualize these findings. In Puglia and Sicilia, severe degradation is likely linked to rising temperatures and declining precipitation, conditions that also affect the southern part of Veneto. Sicilia also exhibits low biomass availability, while Puglia and the Northern regions (especially Emilia-Romagna and Veneto) show high livestock densities and water stress, which is also very critical in

Sicilia. Lastly, the Po Valley in Emilia-Romagna, along with parts of Puglia and Sicilia, are frequently exposed to bare soil conditions, compounding degradation risks.

5. Conclusions

This article introduces RURALIS, a remote sensing-based multi-model framework presenting a flexible, scalable, and context-aware approach tailored to Italy rural landscapes. RURALIS builds on the central role of satellite remote sensing to produce spatially detailed outputs and deliver actionable insights for more effective rural land management.

By adopting a model-learning strategy inspired by reverse engineering, this work analyzes the structure and logic of three established LD models and synthesizes their most relevant features into an integrated framework. The resulting RURALIS model incorporates key indicators of vegetation condition, human pressure, and land dynamics, producing a spatially detailed degradation index that aligns with the realities of agricultural and livestock-intensive environments.

According to its outputs, more than half of Italy's rural areas are at risk of degradation, around 30% are lightly degraded, and less than 10% are classified as severely degraded.

To strengthen the robustness of these findings and address quantitative validation limitations, a Random Forest classification was applied to identify areas of consensus across the methodologies and to produce a robust, integrated degradation map.

The Random Forest model identified approximately 2.34 million hectares (13.6%) of rural land in Italy as severely degraded. The most affected areas include northern Puglia and Sicilia, with degradation patterns in northern Italy appearing more spatially homogeneous, particularly in Emilia-Romagna, Lombardia, and Veneto. These spatial insights, supported by temporal evidence from the RURALIS model, highlight the influence of increasing temperatures, water stress, biomass loss, and agricultural pressure in driving degradation processes.

Beyond its scientific contributions, the model also serves as a practical decision-support tool for regional monitoring and planning. It demonstrates the potential of remote sensing to support more dynamic and spatially explicit LD assessments. Importantly, it underscores the need for regular updates based on robust, remote-sensing-derived indicators to assess not only degradation dynamics but also the effectiveness of policies and land management interventions.

Future developments will focus on addressing validation and computational demand challenges and integrating additional indicators such as Above-Ground Biomass (AGB), which may provide a more consistent measure of vegetation productivity than current proxies like NPP. Ultimately, RURALIS offers a flexible, evidence-based foundation for monitoring land degradation in rural contexts and contributes to bridging the gap between high-resolution earth observation data and policy-relevant environmental assessments.

Supplementary Materials: The following supporting information can be downloaded at: https://www.mdpi.com/article/10.3390/rs17193276/s1, Table S1: RURALIS weighting system for each indicator across the 32 sub-regional tiles; Figure S1: Dominant indicators identified by RURALIS across the 32-tile system; Figure S2: Environmental sensitive areas index classification, where N = Not affected; P = Potentially Affected; F1, F2, F3 = Fragile; C1, C2, C3 = Critical (2.a). Environmental critical factors classification (b), where 0 = no critical factors; $\geq$8 = at least 8 critical factors (2.b). 250-m resolution; Figure S3: Percentage of Area by Region and Class–Heatmap; Figure S4: SDG Indicator 15.3.1 Land degradation map of rural areas (4.a), where D = Degradation; S = Stable; I = Improvement; SDG Indicator 15.3.1 Land degradation type (4.b), where P = Persistent; R = Recent; I = Improved. 30-m resolution; Figure S5: SDG Indicator 15.3.1 Percentage of area per class and region–Heatmap; Figure S6. DDI classification of Albedo-MSAVI (6.a), Albedo-NDVI (6.b) and Albedo-RVI (6.c) where NC = No change; SR = Slight restoration; MR = Marked restoration;

SD = Slight Degradation; MD = Marked Degradation. 25.8 m resolution. The tiling effect observed in the maps arises from the sub-division of the study area into 32 grid tiles, a procedure adopted to optimize computational processing. Moreover, the random sampling of points for classification and analysis may have con-tributed to amplifying the visibility of this effect; Figure S7: Albedo-MSAVI model—Percentage of area per class and region–Heatmap; Figure S8: Albedo-NDVI model - Percentage of area per class and region–Heatmap; Figure S9: Albedo-RVI model-Percentage of area per class and region–Heatmap

Author Contributions: Conceptualization, F.D. and A.P.; methodology, F.D., O.D., N.R., F.M., F.I. and A.P.; software, F.D., N.R. and F.I.; validation, F.M. and O.D.; formal analysis, F.D. and A.P.; investigation, F.D. and A.P.; resources, A.P.; data curation, F.D.; writing—original draft preparation, F.D. and A.P.; writing—review and editing, O.D. and F.M.; visualization, F.M.; supervision, A.P.; project administration, A.P.; funding acquisition, A.P. All authors have read and agreed to the published version of the manuscript.

Funding: The work of O.D. and N.R., was supported by the European Union's Horizon—MSCA-SE-2021 Research and Innovation Programme under the Marie Sklodowvska-Curie EWALKD_Grant Agreement 10108625.

Data Availability Statement: The data presented in this study are available on request from the corresponding author. The data are not publicly available due to the large amount of data.

Conflicts of Interest: The authors declare no conflicts of interest.

Abbreviations

The following abbreviations are used in this manuscript:

AHP	Analytical Hierarchical Process
AI	Aridity Index
CASA	Carnegie-Ames-Stanford Approach
CCI	Climate Change Initiative
CHRIPS	Climate Hazards Group InfraRed Precipitation with Station
CLC	CORINE Land Cover
CO_2	Carbon Dioxide
CQI	Climate Quality Index
CR	Consistency Ratio
CRS	Coordinate Reference System
DDI	Degradation Difference Index
ECF	Environmental Critical Factor
EEI	Evapotranspiration Efficiency Index
ELT	Extract, Load and Transform
ESAI	Environmentally Sensitive Area Index
ET	Evapotranspiration
FAPAR	Fraction of Absorbed Photosynthetically Active Radiation
FCOVER	Fraction of Vegetation Cover
FLU	Factor associated with Land Use
FNF	Forest/Non-Forest
GAUL	Global Administrative Unit Layers
GEE	Google Earth Engine
GIS	Geographic Information System
GPP	Gross Primary Productivity
HWSD	Harmonized World Soil Database
IDI	Integrated Desertification Index
IPCC	Intergovernmental Panel on Climate Change
ISPRA	Istituto Superiore per la Protezione e la Ricerca Ambientale
ISTAT	Istituto Nazionale di Statistica

JRC	Joint Research Centre
LAI	Leaf Area Index
LD	Land Degradation
LDDI	Land Degradation Development Index
LDN	Land Degradation Neutrality
LDSI	Land Degradation Status Index
LMI	Land Multi-Degradation Index
LST	Land Surface Temperature
MEDALUS	MEditerranean Desertification And Land USe
MQI	Management Quality Index
MSAVI	Modified Soil Adjusted Vegetation Index
MSI	MultiSpectral Instrument
NDVI	Normalized Difference Vegetation Index
NPP	Net Primary Productivity
OSM	OpenStreetMap
PET	Potential Evapotranspiration
RALDE	Risk Assessment of Land Degradation
RF	Random Forest
RS	Remote Sensing
RUE	Rainfall Use Efficiency
RURALIS	RURal Areas Land Degradation Indicator System
RVI	Radar Vegetation Index
SAR	Synthetic Aperture Radar
SAVI	Soil Adjusted Vegetation Index
SDG	Sustainable Development Goals
SEPAL	System for Earth Observation Data Access, Processing and Analysis for Land Monitoring
SNAP	Sentinel Application Platform
SNPA	National System for Environmental Protection
SOC	Soil Organic Carbon
SQI	Soil Quality Index
TSEB	Two-Source Energy Balance
UAA	Utilized Agricultural Area
UN	United Nations
UNCCD	United Nations Convention to Combat Desertification
USLE	Universal Soil Loss Equation
VQI	Vegetation Quality Index
WLC	Weighted Linear Combination
WUE	Water Use Efficiency

References

1. UNCCD. *Elaboration of an International Convention to Combat Desertification in Countries Experiencing Serious Drought and/or Desertification, Particularly in Africa*; UN: Bonn, Germany, 1994.
2. Santarsiero, V.; Nolè, G.; Lanorte, A.; Murgante, B. Towards Quantifying Rural Environment Soil Erosion: RUSLE Model and Remote Sensing Based Approach in Basilicata (Southern Italy). In *New Metropolitan Perspectives*; Calabrò, F., Della Spina, L., Piñeira Mantiñán, M.J., Eds.; Lecture Notes in Networks and Systems; Springer International Publishing: Cham, Switzerland, 2022; Volume 482, pp. 2163–2172, ISBN 978-3-031-06824-9.
3. Warren, A. Land Degradation Is Contextual. *Land Degrad. Dev.* **2002**, *13*, 449–459. [CrossRef]
4. Sengani, D.; Ramoelo, A.; Archer, E. A Review of Fusion Framework Using Optical Sensors and Synthetic Aperture Radar Imagery to Detect and Map Land Degradation and Sustainable Land Management in the Semi-Arid Regions. *Geocarto Int.* **2023**, *38*, 2278325. [CrossRef]
5. Prăvălie, R.; Borrelli, P.; Panagos, P.; Ballabio, C.; Lugato, E.; Chappell, A.; Miguez-Macho, G.; Maggi, F.; Peng, J.; Niculiță, M.; et al. A Unifying Modelling of Multiple Land Degradation Pathways in Europe. *Nat. Commun.* **2024**, *15*, 3862. [CrossRef]

6. Previtali, M. A GIS and Remote Sensing Approach for Desertification Sensitivity Assessment of Cultural Landscape in Apulia Region (Italy). In *Digital Heritage. Progress in Cultural Heritage: Documentation, Preservation, and Protection*; Ioannides, M., Fink, E., Cantoni, L., Champion, E., Eds.; Lecture Notes in Computer Science; Springer International Publishing: Cham, Switzerland, 2021; Volume 12642, pp. 138–149, ISBN 978-3-030-73042-0.
7. Schröter-Schlaack, C.; Albert, C.; von Haaren, C.; Hansjürgens, B.; Krätzig, S.; Albert, I. *Ecosystem Services in Rural Areas: Basis for Human Wellbeing and Sustainable Economic Development: Summary for Decision-Makers*; Naturkapital Deutschland—TEEB DE: Hannover, Germany; Leipzig, Germany, 2016; ISBN 978-3-944280-21-9.
8. Power, A.G. Ecosystem Services and Agriculture: Tradeoffs and Synergies. *Philos. Trans. R. Soc. B Biol. Sci.* **2010**, *365*, 2959–2971. [CrossRef] [PubMed]
9. D'Acunto, F.; Marinello, F.; Pezzuolo, A. Rural Land Degradation Assessment through Remote Sensing: Current Technologies, Models, and Applications. *Remote Sens.* **2024**, *16*, 3059. [CrossRef]
10. Costa, D.P.; Herrmann, S.M.; Vasconcelos, R.N.; Duverger, S.G.; Franca Rocha, W.J.S.; Cambuí, E.C.B.; Lobão, J.S.B.; Santos, E.M.R.; Ferreira-Ferreira, J.; Oliveira, M.; et al. Bibliometric Analysis of Land Degradation Studies in Drylands Using Remote Sensing Data: A 40-Year Review. *Land* **2023**, *12*, 1721. [CrossRef]
11. Kang, J.; Zhang, Y.; Biswas, A. Land Degradation and Development Processes and Their Response to Climate Change and Human Activity in China from 1982 to 2015. *Remote Sens.* **2021**, *13*, 3516. [CrossRef]
12. Lamaamri, M.; Lghabi, N.; Ghazi, A.; El Harchaoui, N.; Adnan, M.S.G.; Shakiul Islam, M. Evaluation of Desertification in the Middle Moulouya Basin (North-East Morocco) Using Sentinel-2 Images and Spectral Index Techniques. *Earth Syst. Environ.* **2023**, *7*, 473–492. [CrossRef]
13. Kimura, R.; Moriyama, M. Determination by MODIS Satellite-Based Methods of Recent Global Trends in Land Surface Aridity and Degradation. *J. Agric. Meteorol.* **2019**, *75*, 153–159. [CrossRef]
14. Kirui, O.K.; Mirzabaev, A.; Von Braun, J. Assessment of Land Degradation 'on the Ground' and from 'Above'. *SN Appl. Sci.* **2021**, *3*, 318. [CrossRef]
15. Ramírez-Juidias, E.; Madueño-Luna, A.; Madueño-Luna, J.M.; López-Gordillo, M.C.; Leiva-Piedra, J.L. Applying Remote Sensing Methods to Estimate Alterations in Land Cover Change and Degradation in the Desert Regions of the Southeast Iberian Peninsula. *Remote Sens.* **2023**, *15*, 3984. [CrossRef]
16. Adesina, E.A.; Muhammad, H.I. Assessment of Land Degradation Using Remote Sensing Approach. *Geod. Cartogr.* **2023**, *49*, 142–148. [CrossRef]
17. Abdi, B.; Kolo, K.; Shahabi, H. Soil Erosion and Degradation Assessment Integrating Multi-Parametric Methods of RUSLE Model, RS, and GIS in the Shaqlawa Agricultural Area, Kurdistan Region, Iraq. *Environ. Monit. Assess.* **2023**, *195*, 1149. [CrossRef] [PubMed]
18. Makhamreh, Z.M. Land Degradation Vulnerability Assessment Based on Land Use Changes and FAO Suitability Analysis in Jordan. *Span. J. Soil Sci.* **2019**, *9*, 3900. [CrossRef]
19. Afifi, A.A.; El Semary, M.A. The Impact of Long Term Cropping and Land Use Change on the Degradation of Heavy Clay Soils in the Nile Delta, Egypt. *Model. Earth Syst. Environ.* **2018**, *4*, 805–814. [CrossRef]
20. Kosmas, C.; Kirkby, M.J.; Geeson, N. *The Medalus Project: Mediterranean Desertification and Land Use, Manual on Key Indicators of Desertification and Mapping Environmentally Sensitive Areas to Desertification*; Office for Official Publications of the European Communities: Luxembourg, 1999; ISBN 978-92-828-6349-7.
21. Masoudi, M.; Vahedi, M.; Cerdà, A. Risk Assessment of Land Degradation (RALDE) Model. *Land Degrad. Dev.* **2021**, *32*, 2861–2874. [CrossRef]
22. AbdelRahman, M.A.E.; Natarajan, A.; Hegde, R.; Prakash, S.S. Assessment of Land Degradation Using Comprehensive Geo-statistical Approach and Remote Sensing Data in GIS-Model Builder. *Egypt. J. Remote Sens. Space Sci.* **2019**, *22*, 323–334. [CrossRef]
23. Sun, B.; Li, Z.; Gao, Z.; Guo, Z.; Wang, B.; Hu, X.; Bai, L. Grassland Degradation and Restoration Monitoring and Driving Forces Analysis Based on Long Time-Series Remote Sensing Data in Xilin Gol League. *Acta Ecol. Sin.* **2017**, *37*, 219–228. [CrossRef]
24. Wang, Y.; Guo, E.; Kang, Y.; Ma, H. Assessment of Land Desertification and Its Drivers on the Mongolian Plateau Using Intensity Analysis and the Geographical Detector Technique. *Remote Sens.* **2022**, *14*, 6365. [CrossRef]
25. Aldabbagh, Y.A.N.; Shafri, H.Z.M.; Mansor, S.; Ismail, M.H. Desertification Prediction with an Integrated 3D Convolutional Neural Network and Cellular Automata in Al-Muthanna, Iraq. *Environ. Monit. Assess.* **2022**, *194*, 715. [CrossRef]
26. Bär, V.; Akinyemi, F.O.; Ifejika Speranza, C. Land Cover Degradation in the Reference and Monitoring Periods of the SDG Land Degradation Neutrality Indicator for Switzerland. *Ecol. Indic.* **2023**, *151*, 110252. [CrossRef]
27. Iodice, F.; D'Acunto, F.; Bigagli, L. Monitoring Land Degradation from Space. *GI_Forum* **2021**, *1*, 143–149. [CrossRef]
28. Guo, Z.; Xie, Y.; Guo, H.; Zhang, X.; Zhang, X.; Xi, G.; Ma, C.; Duan, H. Is Land Degradation Worsening in Northern China? Quantitative Evidence and Enlightenment from Satellites. *Land Degrad. Dev.* **2023**, *34*, 1662–1680. [CrossRef]

29. Samela, C.; Imbrenda, V.; Coluzzi, R.; Pace, L.; Simoniello, T.; Lanfredi, M. Multi-Decadal Assessment of Soil Loss in a Mediterranean Region Characterized by Contrasting Local Climates. *Land* **2022**, *11*, 1010. [CrossRef]
30. Petito, M.; Cantalamessa, S.; Pagnani, G.; Degiorgio, F.; Parisse, B.; Pisante, M. Impact of Conservation Agriculture on Soil Erosion in the Annual Cropland of the Apulia Region (Southern Italy) Based on the RUSLE-GIS-GEE Framework. *Agronomy* **2022**, *12*, 281. [CrossRef]
31. Panagos, P.; Standardi, G.; Borrelli, P.; Lugato, E.; Montanarella, L.; Bosello, F. Cost of Agricultural Productivity Loss Due to Soil Erosion in the European Union: From Direct Cost Evaluation Approaches to the Use of Macroeconomic Models. *Land Degrad. Dev.* **2018**, *29*, 471–484. [CrossRef]
32. Santarsiero, V.; Lanorte, A.; Nolè, G.; Cillis, G.; Tucci, B.; Murgante, B. Analysis of the Effect of Soil Erosion in Abandoned Agricultural Areas: The Case of NE Area of Basilicata Region (Southern Italy). *Land* **2023**, *12*, 645. [CrossRef]
33. Gabriele, M.; Brumana, R.; Previtali, M.; Cazzani, A. A Combined GIS and Remote Sensing Approach for Monitoring Climate Change-Related Land Degradation to Support Landscape Preservation and Planning Tools: The Basilicata Case Study. *Appl. Geomat.* **2023**, *15*, 497–532. [CrossRef]
34. Leginio, M.D.; Agrillo, A.; Congedo, L.; Munafò, M.; Riitano, N.; Terribile, F.; Manna, P. Analysis of Trends in Productivity Metrics in Assessing Land Degradation: A Case Study in the Campania Region of Southern Italy. *Ecol. Indic.* **2024**, *161*, 111962. [CrossRef]
35. Colombo, R. Assessment of Mediterranean Pasture Condition Using MODIS Normalized Difference Vegetation Index Time Series. *J. Appl. Remote Sens.* **2012**, *6*, 063530. [CrossRef]
36. Cillis, G.; Nolè, G.; Lanorte, A.; Santarsiero, V.; Tucci, B.; Scorza, F.; Murgante, B. Soil Erosion and Land Degradation in Rural Environment: A Preliminary GIS and Remote-Sensed Approach. In *Computational Science and Its Applications—ICCSA 2021*; Gervasi, O., Murgante, B., Misra, S., Garau, C., Blečić, I., Taniar, D., Apduhan, B.O., Rocha, A.M.A.C., Tarantino, E., Torre, C.M., Eds.; Lecture Notes in Computer Science; Springer International Publishing: Cham, Switzerland, 2021; Volume 12954, pp. 682–694, ISBN 978-3-030-86978-6.
37. Tucci, B.; Nolè, G.; Lanorte, A.; Santarsiero, V.; Cillis, G.; Scorza, F.; Murgante, B. Assessment and Monitoring of Soil Erosion Risk and Land Degradation in Arable Land Combining Remote Sensing Methodologies and RUSLE Factors. In *Computational Science and Its Applications—ICCSA 2021*; Gervasi, O., Murgante, B., Misra, S., Garau, C., Blečić, I., Taniar, D., Apduhan, B.O., Rocha, A.M.A.C., Tarantino, E., Torre, C.M., Eds.; Lecture Notes in Computer Science; Springer International Publishing: Cham, Switzerland, 2021; Volume 12954, pp. 704–716, ISBN 978-3-030-86978-6.
38. Basso, F.; Bove, E.; Dumontet, S.; Ferrara, A.; Pisante, M.; Quaranta, G.; Taberner, M. Evaluating Environmental Sensitivity at the Basin Scale through the Use of Geographic Information Systems and Remotely Sensed Data: An Example Covering the Agri Basin (Southern Italy). *Catena* **2000**, *40*, 19–35. [CrossRef]
39. SNPA. *Consumo Di Suolo, Dinamiche Territoriali e Servizi Ecosistemici*, 2024th ed.; [Land Consumption, Spatial Dynamics and Ecosystem Servicesibespoke. 2024 Edition]; Report Ambientali; SNPA: Roma, Italy, 2024.
40. United Nations Statistics Division (UN STATS) SDG Indicator Metadata. Available online: https://unstats.un.org/sdgs/metadata/files/Metadata-15-03-01.pdf (accessed on 9 September 2025).
41. Bissenbayeva, S.; Salmurzauly, R.; Tokbergenova, A.; Zhengissova, N.; Xing, J. Assessment of Degraded Lands in the Ile-Balkhash Region, Kazakhstan. *Front. Earth Sci.* **2025**, *12*, 1453994. [CrossRef]
42. d'Andrimont, R.; Verhegghen, A.; Lemoine, G.; Kempeneers, P.; Meroni, M.; Van Der Velde, M. From Parcel to Continental Scale—A First European Crop Type Map Based on Sentinel-1 and LUCAS Copernicus in-Situ Observations. *Remote Sens. Environ.* **2021**, *266*, 112708. [CrossRef]
43. Shimada, M.; Itoh, T.; Motooka, T.; Watanabe, M.; Shiraishi, T.; Thapa, R.; Lucas, R. New Global Forest/Non-Forest Maps from ALOS PALSAR Data (2007–2010). *Remote Sens. Environ.* **2014**, *155*, 13–31. [CrossRef]
44. Pesaresi, M.; Politis, P. *GHS-BUILT-C R2023A—GHS Settlement Characteristics, Derived from Sentinel2 Composite (2018) and Other GHS R2023A Data*; European Commission: Brussels, Belgium, 2023.
45. Copernicus Sentinel Data 2018. Available online: https://developers.google.com/earth-engine/datasets/catalog/COPERNICUS_S1_GRD (accessed on 1 August 2025).
46. Uptoearth GmbH D3.1 GIS Maps for the Identification of Soil for Biomass 2024. Available online: https://ec.europa.eu/research/participants/documents/downloadPublic?documentIds=080166e51a3b0bc3&appId=PPGMS (accessed on 14 September 2025).
47. Gorelick, N.; Hancher, M.; Dixon, M.; Ilyushchenko, S.; Thau, D.; Moore, R. Google Earth Engine: Planetary-Scale Geospatial Analysis for Everyone. *Remote Sens. Environ.* **2017**, *202*, 18–27. [CrossRef]
48. QGIS.org. *QGIS Geographic Information System*, Version 3.42. Available online: https://qgis.org/ (accessed on 14 September 2025).
49. FAO. *The Global Administrative Unit Layers (GAUL) Dataset, Implemented by FAO within the CountrySTAT and Agricultural Market Information System (AMIS) Projects*; FAO: Rome, Italy, 2024.
50. Python Software Foundation Python Language Reference, Version 3.12.7. Available online: http://www.python.org (accessed on 14 September 2025).

51. Ferrara, A.; Kosmas, C.; Salvati, L.; Padula, A.; Mancino, G.; Nolè, A. Updating the MEDALUS-ESA Framework for Worldwide Land Degradation and Desertification Assessment. *Land Degrad. Dev.* **2020**, *31*, 1593–1607. [CrossRef]
52. Sharma, L.K.; Raj, A.; Somawat, K. Spatio-Temporal Assessment of Environmentally Sensitive Areas (ESA) in The Thar Desert India, to Combat Desertification under UNCCD Framework. *J. Arid Environ.* **2021**, *194*, 104609. [CrossRef]
53. Ouakil, A.; Eddefli, F.; Hichou, B.B.; Chao, J.; Elbelrhiti, H. Integration of Sentinel2 Data into a GIS System for the Mapping of Areas at Risk of Degradation by Applying the MEDALUS Model—Case of Sidi Mohamed Ben Abdellah Watershed (Morocco). Ecol. *Eng. Environ. Technol.* **2023**, *24*, 216–228. [CrossRef]
54. Ouachoua, R.; Al Karkouri, J. Assessing Environmental Sensitivity Areas to Desertification Using MEDALUS Model in Ziz-Rheris Watershed, Morocco. *Int. J. Sci. Res. Multidiscip. Stud.* **2020**, *6*, 18–26.
55. Singh, B.; Cattle, S.R.; Field, D.J. Edaphic Soil Science, Introduction to. In *Encyclopedia of Agriculture and Food Systems*; Elsevier: Amsterdam, The Netherlands, 2014; pp. 35–58, ISBN 978-0-08-093139-5.
56. Bucci, F.; Santangelo, M.; Fongo, L.; Alvioli, M.; Cardinali, M.; Melelli, L.; Marchesini, I. A New Digital Lithological Map of Italy at 1:100.000 Scale; 2 Data Points. 2021. Available online: https://doi.pangaea.de/10.1594/PANGAEA.935673 (accessed on 12 September 2025).
57. Nabiollahi, K.; Golmohamadi, F.; Taghizadeh-Mehrjardi, R.; Kerry, R.; Davari, M. Assessing the Effects of Slope Gradient and Land Use Change on Soil Quality Degradation through Digital Mapping of Soil Quality Indices and Soil Loss Rate. *Geoderma* **2018**, *318*, 16–28. [CrossRef]
58. Farr, T.G.; Rosen, P.A.; Caro, E.; Crippen, R.; Duren, R.; Hensley, S.; Kobrick, M.; Paller, M.; Rodriguez, E.; Roth, L.; et al. The Shuttle Radar Topography Mission. *Rev. Geophys.* **2007**, *45*, 2005RG000183. [CrossRef]
59. *Harmonized World Soil Database*, version 2.0; FAO: Rome, Italy; International Institute for Applied Systems Analysis (IIASA): Laxenburg, Austria, 2023; ISBN 978-92-5-137499-3.
60. Vinhal-Freitas, I.C.; Corrêa, G.F.; Wendling, B.; Bobul'ská, L.; Ferreira, A.S. Soil Textural Class Plays a Major Role in Evaluating the Effects of Land Use on Soil Quality Indicators. *Ecol. Indic.* **2017**, *74*, 182–190. [CrossRef]
61. Colantoni, A.; Ferrara, C.; Perini, L.; Salvati, L. Assessing Trends in Climate Aridity and Vulnerability to Soil Degradation in Italy. *Ecol. Indic.* **2015**, *48*, 599–604. [CrossRef]
62. Funk, C.; Peterson, P.; Landsfeld, M.; Pedreros, D.; Verdin, J.; Shukla, S.; Husak, G.; Rowland, J.; Harrison, L.; Hoell, A.; et al. The Climate Hazards Infrared Precipitation with Stations—A New Environmental Record for Monitoring Extremes. *Sci. Data* **2015**, *2*, 150066. [CrossRef]
63. Nastos, P.T.; Politi, N.; Kapsomenakis, J. Spatial and Temporal Variability of the Aridity Index in Greece. *Atmospheric Res.* **2013**, *119*, 140–152. [CrossRef]
64. Copernicus Climate Change Service (C3S). *ERA5: Fifth Generation of ECMWF Atmospheric Reanalyses of the Global Climate*; Copernicus Climate Change Service Climate Data Store (CDS): Bonn, Germany, 2017.
65. Copernicus Climate Change Service. *Land Cover Classification Gridded Maps from 1992 to Present Derived from Satellite Observations*; Copernicus Climate Change Service: Bonn, Germany, 2019.
66. Hamad, K.O.; Surucu, A. Land Degradation Sensitivity and Desertification Risk in Harrir Region, Northern Iraq. *Heliyon* **2024**, *10*, e27123. [CrossRef]
67. MODIS/Terra Vegetation Indices Monthly L3 Global 1km SIN Grid V061. 2021. Available online: https://developers.google.com/earth-engine/datasets/catalog/MODIS_061_MOD13A3 (accessed on 14 September 2025).
68. Prăvălie, R.; Patriche, C.; Săvulescu, I.; Sîrodoev, I.; Bandoc, G.; Sfîcă, L. Spatial Assessment of Land Sensitivity to Degradation across Romania. A Quantitative Approach Based on the Modified MEDALUS Methodology. *Catena* **2020**, *187*, 104407. [CrossRef]
69. Jafari, R.; Abedi, M. Remote Sensing-based Biological and Nonbiological Indices for Evaluating Desertification in Iran: Image versus Field Indices. *Land Degrad. Dev.* **2021**, *32*, 2805–2822. [CrossRef]
70. Mancebo, F.; Sachs, I. (Eds.) *Transitions to Sustainability*, 1st ed.; Springer Netherlands: Imprint; Springer: Dordrecht, The Netherlands, 2015; ISBN 978-94-017-9532-6.
71. United Nations Department of Economic and Social Affairs (UN DESA). *E-Handbook on Sustainable Development Goals Indicators*; UN DESA: New York, NY, USA, 2024.
72. Di Gregorio, A.; Food and Agriculture Organization of the United Nations (FAO) (Eds.) *Land Cover Classification System: Classification Concepts and User Manual*, Software Version 2; Environment and Natural Resources Series GEO-Spatial Data and Information; Food and Agriculture Organization of the United Nations: Rome, Italy, 2005; ISBN 978-92-5-105327-0.
73. Sims, N.C.; Green, C.; Newnham, G.J.; England, J.R.; Held, A.; Wulder, M.A.; Herold, M.; Guerschman, J.; Cox, S.J.D.; Huete, A.R.; et al. Good Practice Guidance. SDG Indicator 15.3.1, Proportion of Land That Is Degraded Over Total Land Area, Version 1.0. 2017. Available online: https://docs.sepal.io/en/latest/modules/dwn/sdg_indicator.html (accessed on 31 July 2025).
74. Liu, L.; Zhang, X.; Zhao, T. GLC_FCS30D: The First Global 30-m Land-Cover Dynamic Monitoring Product with Fine Classification System from 1985 to 2022. 2023. Available online: https://gee-community-catalog.org/projects/glc_fcs/ (accessed on 1 August 2025).

75. IPCC. *Good Practice Guidance for Land Use, Land-Use Change and Forestry*; Penman, J., Ed.; The Intergovernmental Panel on Climate Change: Hayama, Japan, 2003; ISBN 978-4-88788-003-0.
76. Sims, N.C.; Newnham, G.J.; England, J.R.; Guerschman, J.; Cox, S.J.D.; Roxburgh, S.H.; Viscarra Rossel, R.A.; Fritz, S.; Wheeler, I. Good Practice Guidance. SDG Indicator 15.3.1, Proportion of Land That Is Degraded Over Total Land Area, Version 2.0. 2021. Available online: https://www.unccd.int/resources/manuals-and-guides/good-practice-guidance-sdg-indicator-1531-proportion-land-degraded (accessed on 14 September 2025).
77. Millennium Ecosystem Assessment (Program) (Ed.) *Ecosystems and Human Well-Being: Synthesis*; Island Press: Washington, DC, USA, 2005; ISBN 978-1-59726-040-4.
78. European Commission; Joint Research Centre. *World Atlas of Desertification: Rethinking Land Degradation and Sustainable Land Management*; Publications Office: Luxembourg, 2018.
79. Kiani-Harchegani, M.; Sadeghi, S.H. Practicing Land Degradation Neutrality (LDN) Approach in the Shazand Watershed, Iran. *Sci. Total Environ.* **2020**, *698*, 134319. [CrossRef]
80. Tucker, C.J. Red and Photographic Infrared Linear Combinations for Monitoring Vegetation. *Remote Sens. Environ.* **1979**, *8*, 127–150. [CrossRef]
81. Earth Resources Observation and Science (EROS) Center. *Landsat 4–5 Thematic Mapper Level-2, Collection 2*; Earth Resources Observation and Science (EROS) Center: Sioux Falls, SD, USA, 2020.
82. Earth Resources Observation and Science (EROS) Center. *Landsat 7 Enhanced Thematic Mapper Plus Level-2, Collection 2*; Earth Resources Observation and Science (EROS) Center: Sioux Falls, SD, USA, 1999.
83. Earth Resources Observation and Science (EROS) Center. *Landsat 8–9 Operational Land Imager/Thermal Infrared Sensor Level-2, Collection 2*; Earth Resources Observation and Science (EROS) Center: Sioux Falls, SD, USA, 2013.
84. Reith, J.; Ghazaryan, G.; Muthoni, F.; Dubovyk, O. Assessment of Land Degradation in Semiarid Tanzania—Using Multiscale Remote Sensing Datasets to Support Sustainable Development Goal 15.3. *Remote Sens.* **2021**, *13*, 1754. [CrossRef]
85. Cherif, I.; Kolintziki, E.; Alexandridis, T.K. Monitoring of Land Degradation in Greece and Tunisia Using Trends.Earth with a Focus on Cereal Croplands. *Remote Sens.* **2023**, *15*, 1766. [CrossRef]
86. Eggleston, H.S. (Ed.) *2006 IPCC Guidelines for National Greenhouse Gas Inventories*; Institute for Global Environmental Strategies: Hayama, Japan, 2006; ISBN 978-4-88788-032-0.
87. Hengl, T.; Wheeler, I. Soil Organic Carbon Content in x 5 g/Kg at 6 Standard Depths (0, 10, 30, 60, 100 and 200 Cm) at 250 m Resolution. 2018. Available online: https://developers.google.com/earth-engine/datasets/catalog/OpenLandMap_SOL_SOL_ORGANIC-CARBON_USDA-6A1C_M_v02 (accessed on 11 September 2025).
88. Trends.Earth. Conservation International Trends.Earth—User Guide, Version 2.17. 2025. Available online: https://docs.trends.earth/en/latest/for_users/index.html (accessed on 14 September 2025).
89. Minelli, S. UNCCD 2018 Default Data: Methods and Interpretation for Land Degradation Reporting. 2018. Available online: https://policycommons.net/artifacts/1983874/default-data/2735639/ (accessed on 8 September 2025).
90. Kottek, M.; Grieser, J.; Beck, C.; Rudolf, B.; Rubel, F. World Map of the Köppen-Geiger Climate Classification Updated. *Meteorol. Z.* **2006**, *15*, 259–263. [CrossRef]
91. Guo, B.; Wei, C.; Yu, Y.; Liu, Y.; Li, J.; Meng, C.; Cai, Y. The Dominant Influencing Factors of Desertification Changes in the Source Region of Yellow River: Climate Change or Human Activity? *Sci. Total Environ.* **2022**, *813*, 152512. [CrossRef] [PubMed]
92. Jia, H.; Wang, R.; Li, H.; Diao, B.; Zheng, H.; Guo, L.; Liu, L.; Liu, J. The Changes of Desertification and Its Driving Factors in the Gonghe Basin of North China over the Past 10 Years. *Land* **2023**, *12*, 998. [CrossRef]
93. Yue, Y.; Li, M.; Zhu, A.; Ye, X.; Mao, R.; Wan, J.; Dong, J. Land Degradation Monitoring in the Ordos Plateau of China Using an Expert Knowledge and BP-ANN-Based Approach. *Sustainability* **2016**, *8*, 1174. [CrossRef]
94. Wu, Z.; Lei, S.; Bian, Z.; Huang, J.; Zhang, Y. Study of the Desertification Index Based on the Albedo-MSAVI Feature Space for Semi-Arid Steppe Region. *Environ. Earth Sci.* **2019**, *78*, 232. [CrossRef]
95. Qi, J.; Chehbouni, A.; Huete, A.R.; Kerr, Y.H.; Sorooshian, S. A Modified Soil Adjusted Vegetation Index. *Remote Sens. Environ.* **1994**, *48*, 119–126. [CrossRef]
96. Belhadj, A.; Boulghobra, N.; Demnati Allache, F. Multi-Temporal Landsat Imagery and MSAVI Index for Monitoring Rangeland Degradation in Arid Ecosystem, Case Study of Biskra (Southeast Algeria). *Environ. Monit. Assess.* **2023**, *195*, 656. [CrossRef]
97. Hu, X.; Li, L.; Huang, J.; Zeng, Y.; Zhang, S.; Su, Y.; Hong, Y.; Hong, Z. Radar Vegetation Indices for Monitoring Surface Vegetation: Developments, Challenges, and Trends. *Sci. Total Environ.* **2024**, *945*, 173974. [CrossRef]
98. Dinesh Kumar, S.; Sitiraju, S.; Sharma, J. Radar Vegetation Index as an Alternative to NDVI for Monitoring of Soyabean and Cotton; Indian Cartographer. 2013. Available online: https://www.academia.edu/50102296/Radar_Vegetation_Index_as_an_Alternative_to_NDVI_for_Monitoring_of_Soyabean_and_Cotton (accessed on 14 September 2025).
99. Chiesi, M.; Angeli, L.; Battista, P.; Fibbi, L.; Rapi, B.; Gozzini, B.; Maselli, F. Monitoring and Analysis of Crop Irrigation Dynamics in Central Italy through the Use of MODIS NDVI Data. *Eur. J. Remote Sens.* **2022**, *55*, 23–36. [CrossRef]

100. Palacios-Orueta, A.; Khanna, S.; Litago, J.; Whiting, M.L.; Ustin, S.L. Assessment of NDVI and NDWI Spectral Indices Using MODIS Time Series Analysis and Development of a New Spectral Index Based on MODIS Shortwave Infrared Bands. In Proceedings of the 1st International Conference on Remote Sensing and Geoinformation Processing in the Assessment and Monitoring of Land Degradation and Desertification, Trier, Germany, 7–9 September 2005. [CrossRef]
101. Thrasher, B.; Maurer, E.P.; McKellar, C.; Duffy, P.B. Technical Note: Bias Correcting Climate Model Simulated Daily Temperature Extremes with Quantile Mapping. *Hydrol. Earth Syst. Sci.* **2012**, *16*, 3309–3314. [CrossRef]
102. Hungate, B.A.; Koch, G.W. GLOBAL CHANGE | Biospheric Impacts and Feedbacks. In *Encyclopedia of Atmospheric Sciences*; Elsevier: Amsterdam, The Netherlands, 2003; pp. 876–886, ISBN 978-0-12-227090-1.
103. Mehta, A.; Shukla, S.; Rakholia, S. Vegetation Change Analysis Using Normalized Difference Vegetation Index and Land Surface Temperature in Greater Gir Landscape. *J. Sci. Res.* **2021**, *65*, 01–06. [CrossRef]
104. Bashar, A.; Haque, I.; Parvin, A.; Hossain, A. Water and Vegetation Cover Change Detection Using Multispectral Satellite Imagery: A Case Study on Jhenaidah District of Bangladesh. *Bangladesh J. Multidiscip. Sci. Res.* **2023**, *7*, 22–34. [CrossRef]
105. How to Reverse Engineer DNA and Quantum Bio-Attacks. In *Biomedical Defense Principles to Counter DNA Deep Hacking*; Elsevier: Amsterdam, The Netherlands, 2023; pp. 307–331, ISBN 978-0-323-99914-4.
106. Kolios, S.; Mitrakos, S.; Stylios, C. Detection of Areas Susceptible to Land Degradation in Cyprus Using Remote Sensed Data and Environmental Quality Indices. *Land Degrad. Dev.* **2018**, *29*, 2338–2350. [CrossRef]
107. Wijitkosum, S. Factor Influencing Land Degradation Sensitivity and Desertification in a Drought Prone Watershed in Thailand. *Int. Soil Water Conserv. Res.* **2021**, *9*, 217–228. [CrossRef]
108. Cudlín, O.; Pechanec, V.; Prokopová, M.; Cudlín, P. Assessing the Vulnerability to Land Degradation of (Not Only) Rural Landscapes Using the ESAI Index. *J. Landsc. Ecol.* **2021**, *14*, 128–144. [CrossRef]
109. Ren, Y.; Liu, X.; Zhang, B.; Chen, X. Sensitivity Assessment of Land Desertification in China Based on Multi-Source Remote Sensing. *Remote Sens.* **2023**, *15*, 2674. [CrossRef]
110. Giordano, L.; Giordano, F.; Grauso, S.; Iannetta, M.; Sciortino, M.; Rossi, L.; Bonati, G. *Identification of Areas Sensitive to Desertification in Sicily Region*; ENEA: Rome, Italy, 2001.
111. SEPAL. SDG Indicator 15.3.1 Module. Available online: https://docs.sepal.io/en/latest/modules/dwn/sdg_indicator.html#user-guide (accessed on 9 September 2025).
112. Sims, N.C.; Barger, N.N.; Metternicht, G.I.; England, J.R. A Land Degradation Interpretation Matrix for Reporting on UN SDG Indicator 15.3.1 and Land Degradation Neutrality. *Environ. Sci. Policy* **2020**, *114*, 1–6. [CrossRef]
113. Xoxo, S.; Mantel, S.; De Vos, A.; Mahlaba, B.; Le Maître, D.; Tanner, J. Towards SDG 15.3: The Biome Context as the Appropriate Degradation Monitoring Dimension. *Environ. Sci. Policy* **2022**, *136*, 400–412. [CrossRef]
114. Giuliani, G.; Chatenoux, B.; Benvenuti, A.; Lacroix, P.; Santoro, M.; Mazzetti, P. Monitoring Land Degradation at National Level Using Satellite Earth Observation Time-Series Data to Support SDG15—Exploring the Potential of Data Cube. *Big Earth Data* **2020**, *4*, 3–22. [CrossRef]
115. Zhao, L.; Jia, K.; Liu, X.; Li, J.; Xia, M. Assessment of Land Degradation in Inner Mongolia between 2000 and 2020 Based on Remote Sensing Data. *Geogr. Sustain.* **2023**, *4*, 100–111. [CrossRef]
116. Lamqadem, A.; Saber, H.; Pradhan, B. Quantitative Assessment of Desertification in an Arid Oasis Using Remote Sensing Data and Spectral Index Techniques. *Remote Sens.* **2018**, *10*, 1862. [CrossRef]
117. Wei, H.; Wang, J.; Cheng, K.; Li, G.; Ochir, A.; Davaasuren, D.; Chonokhuu, S. Desertification Information Extraction Based on Feature Space Combinations on the Mongolian Plateau. *Remote Sens.* **2018**, *10*, 1614. [CrossRef]
118. Allen, R.G.; Food and Agriculture Organization of the United Nations (Eds.) *Crop Evapotranspiration: Guidelines for Computing Crop Water Requirements*; FAO Irrigation and Drainage Paper; Food and Agriculture Organization of the United Nations: Rome, Italy, 1998; ISBN 978-92-5-104219-9.
119. Biggs, T.W.; Nagler, P.L.; Ruhoff, A.; Petsini, T.; Marshall, M.; Kagone, S.; Senay, G.B.; Petropoulos, G.P.; Abe, C.; Glenn, E.P. Remote Sensing of Evapotranspiration from Croplands. In *Remote Sensing Handbook, Volume V*; CRC Press: Boca Raton, FL, USA, 2024; pp. 313–382, ISBN 978-1-003-54140-0.
120. Technical Committee on Standardization of Reference Evapotranspiration. *The ASCE Standardized Reference Evapotranspiration Equation*; Allen, R.G., Walter, I.A., Elliott, R.L., Howell, T.A., Itenfisu, D., Jensen, M.E., Snyder, R.L., Eds.; American Society of Civil Engineers: Reston, VA, USA, 2005; ISBN 978-0-7844-0805-6.
121. Norman, J.M.; Kustas, W.P.; Humes, K.S. A Two-Source Approach for Estimating Soil and Vegetation Energy Fluxes from Observations of Directional Radiometric Surface Temperature. *Agric. For. Meteorol.* **1995**, *77*, 263–293. [CrossRef]
122. Guzinski, R.; Nieto, H.; Sandholt, I.; Karamitilios, G. Modelling High-Resolution Actual Evapotranspiration through Sentinel-2 and Sentinel-3 Data Fusion. *Remote Sens.* **2020**, *12*, 1433. [CrossRef]
123. DHI GRAS; IRTA; Sandholt ApS. User Manual for SEN-ET SNAP Plugin. 2020. Available online: https://www.esa-sen4et.org/static/media/sen-et-user-manual-v1.1.0.2cd617fb322658397542.pdf (accessed on 1 September 2025).

124. Ghassemi, B.; Dujakovic, A.; Żółtak, M.; Immitzer, M.; Atzberger, C.; Vuolo, F. Designing a European-Wide Crop Type Mapping Approach Based on Machine Learning Algorithms Using LUCAS Field Survey and Sentinel-2 Data. *Remote Sens.* **2022**, *14*, 541. [CrossRef]
125. Bausch, W.C.; Neale, C.M. Crop Coefficients Derived from Reflected Canopy Radiation: A Concept. *Trans. ASAE* **1987**, *30*, 0703–0709. [CrossRef]
126. Idrisa, H.; Kadam, S.A.; Gorantiwar, S.D. Estimation of Crop Coefficients Based on Normalize Difference Vegetation Index. *J. Agric. Res. Technol.* **2022**, *47*, 381–388. [CrossRef]
127. Kamble, B.; Kilic, A.; Hubbard, K. Estimating Crop Coefficients Using Remote Sensing-Based Vegetation Index. *Remote Sens.* **2013**, *5*, 1588–1602. [CrossRef]
128. Weiss, M.; Baret, F. S2ToolBox Level 2 Products: LAI, FAPAR, FCOVER; Algorithm Theoretical Basis Document. 2016. Available online: https://step.esa.int/docs/extra/ATBD_S2ToolBox_L2B_V1.1.pdf (accessed on 1 September 2025).
129. Copernicus Climate Change Service. *ERA5-Land Monthly Averaged Data from 1950 to Present*; Copernicus Climate Change Service: Bonn, Germany, 2019.
130. Poggio, L.; De Sousa, L.M.; Batjes, N.H.; Heuvelink, G.B.M.; Kempen, B.; Ribeiro, E.; Rossiter, D. SoilGrids 2.0: Producing Soil Information for the Globe with Quantified Spatial Uncertainty. *Soil* **2021**, *7*, 217–240. [CrossRef]
131. Chan, S.K.; Bindlish, R.; O'Neill, P.; Jackson, T.; Njoku, E.; Dunbar, S.; Chaubell, J.; Piepmeier, J.; Yueh, S.; Entekhabi, D.; et al. Development and Assessment of the SMAP Enhanced Passive Soil Moisture Product. *Remote Sens. Environ.* **2018**, *204*, 931–941. [CrossRef] [PubMed]
132. Nzuza, P.; Ramoelo, A.; Odindi, J.; Kahinda, J.M.; Madonsela, S. Predicting Land Degradation Using Sentinel-2 and Environmental Variables in the Lepellane Catchment of the Greater Sekhukhune District, South Africa. *Phys. Chem. Earth Parts ABC* **2021**, *124*, 102931. [CrossRef]
133. Masuku, S.N.; Mabaso, S.D. Land Use and Land Cover Change Analysis and Soil Erosion Assessment Using GIS and Remote Sensing in Nkonjwa Community, Eswatini. 2024. Available online: https://www.authorea.com/users/856403/articles/1240845-land-use-and-land-cover-change-analysis-and-soil-erosion-assessment-using-gis-and-remote-sensing-in-nkonjwa-community-eswatini (accessed on 12 September 2025).
134. Zhao, J.; Du, D.; Chen, L.; Liang, X.; Chen, H.; Jin, Y. HA-Net for Bare Soil Extraction Using Optical Remote Sensing Images. *Remote Sens.* **2024**, *16*, 3088. [CrossRef]
135. Ragasová, L.; Kopta, T.; Winkler, J.; Pokluda, R. The Current Stage of Greening Vegetation in Selected Wine-Regions of South Moravian Region (Czech Republic). *Agronomy* **2019**, *9*, 541. [CrossRef]
136. Lal, R. Soil Degradation by Erosion. *Land Degrad. Dev.* **2001**, *12*, 519–539. [CrossRef]
137. Huang, S.; Islam, M.U.; Jiang, F. The Effect of Deep-Tillage Depths on Crop Yield: A Global Meta-Analysis. *Plant Soil Environ.* **2023**, *69*, 105–117. [CrossRef]
138. Cheng, B.; Dai, H.; Liu, T.; Liu, H.; Li, J.; Qiao, R.; Shao, Y.; Wang, S.; Wang, J. Mineralization Characteristics of Soil Organic Carbon under Different Herbaceous Plant Mosaics in Semi-Arid Grasslands. *Sci. Rep.* **2024**, *14*, 22196. [CrossRef]
139. Lal, R. Restoring Soil Quality to Mitigate Soil Degradation. *Sustainability* **2015**, *7*, 5875–5895. [CrossRef]
140. Mzid, N.; Pignatti, S.; Huang, W.; Casa, R. An Analysis of Bare Soil Occurrence in Arable Croplands for Remote Sensing Topsoil Applications. *Remote Sens.* **2021**, *13*, 474. [CrossRef]
141. Satalino, G.; Mattia, F.; Balenzano, A.; Lovergine, F.P.; Rinaldi, M.; De Santis, A.P.; Ruggieri, S.; Nafria Garcia, D.A.; Gomez, V.P.; Ceschia, E.; et al. Sentinel-1 & Sentinel-2 Data for Soil Tillage Change Detection. In Proceedings of the IGARSS 2018—2018 IEEE International Geoscience and Remote Sensing Symposium, Valencia, Spain, 22–27 July 2018; pp. 6627–6630.
142. Steinfeld, H.; Gerber, P.; Wassenaar, T.D.; Castel, V.; Rosales, M.M.; de Haan, C. *Livestock's Long Shadow: Environmental Issues and Options*; Food and Agriculture Organization of the United Nations: Rome, Italy, 2006; ISBN 978-92-5-105571-7.
143. Avondo, M.; Secchiari, P.; Battaglini, L.M.; Bonanno, A.; Pulina, G. Soil, Pasture and Animal Product Quality. *Ital. J. Agron.* **2013**, *8*, e19. [CrossRef]
144. Parvage, M.M.; Ulén, B.; Kirchmann, H. Nutrient Leaching from Manure-Amended Topsoils (Cambisols and Histosols) in Sweden. *Geoderma Reg.* **2015**, *5*, 209–214. [CrossRef]
145. Pulina, G.; Zucca, C. Un Nuovo Indicatore Territoriale per La Valutazione Dell'impatto Del Pascolamento. *Inf. Agrar.* **1999**, *42/99*, 105–110.
146. Gabriele, M.; Previtali, M. A GIS and Remote Sensing Approach for Desertification Sensitivity Assessment in Basilicata Region (Italy). In Proceedings of the 2020 3rd International Conference on Geoinformatics and Data Analysis, Marseille, France, 15 April 2020; ACM: New York, NY, USA; pp. 62–66.
147. Istituto Nazionale di Statistica (Istat). *Confini Delle Unità Amministrative a Fini Statistici 2024 [Boundaries of Administrative Units for Statistical Purposes 2024]*; Istituto Nazionale di Statistica (Istat): Roma, Italy, 2018.
148. Cozzi, G.; Ragno, E. Meat Production and Market in Italy. *Agric. Conspec. Sci.* **2003**, *68*, 71–77.

149. Eurostat Livestock Unit (LSU). Available online: https://ec.europa.eu/eurostat/statistics-explained/index.php?title=Glossary:Livestock_unit_(LSU) (accessed on 1 August 2025).
150. Running, S.; Zhao, M. MODIS/Terra Net Primary Production Gap-Filled Yearly L4 Global 500m SIN Grid V061. 2021. Available online: https://developers.google.com/earth-engine/datasets/catalog/MODIS_061_MOD17A3HGF (accessed on 1 August 2025).
151. Yadav, B.; Malav, L.C.; Jiménez-Ballesta, R.; Kumawat, C.; Patra, A.; Patel, A.; Jangir, A.; Nogiya, M.; Meena, R.L.; Moharana, P.C.; et al. Modeling and Assessment of Land Degradation Vulnerability in Arid Ecosystem of Rajasthan Using Analytical Hierarchy Process and Geospatial Techniques. *Land* **2022**, *12*, 106. [CrossRef]
152. Malczewski, J. On the Use of Weighted Linear Combination Method in GIS: Common and Best Practice Approaches. *Trans. GIS* **2000**, *4*, 5–22. [CrossRef]
153. Yang, Y.; Song, G.; Lu, S. Assessment of Land Ecosystem Health with Monte Carlo Simulation: A Case Study in Qiqihaer, China. *J. Clean. Prod.* **2020**, *250*, 119522. [CrossRef]
154. Gao, H. Agricultural Soil Data Analysis Using Spatial Clustering Data Mining Techniques. In Proceedings of the 2021 IEEE 13th International Conference on Computer Research and Development (ICCRD), Beijing, China, 5 January 2021; pp. 83–90.
155. Salvati, L.; Smiraglia, D.; Bajocco, S.; Ceccarelli, T.; Zitti, M.; Perini, L. Map of Long-Term Changes in Land Sensitivity to Degradation of Italy. *J. Maps* **2014**, *10*, 65–72. [CrossRef]
156. Kennard, M.J.; Mackay, S.J.; Pusey, B.J.; Olden, J.D.; Marsh, N. Quantifying Uncertainty in Estimation of Hydrologic Metrics for Ecohydrological Studies. *River Res. Appl.* **2010**, *26*, 137–156. [CrossRef]
157. Panagos, P.; Broothaerts, N.; Ballabio, C.; Orgiazzi, A.; De Rosa, D.; Borrelli, P.; Liakos, L.; Vieira, D.; Van Eynde, E.; Arias Navarro, C.; et al. How the EU Soil Observatory Is Providing Solid Science for Healthy Soils. *Eur. J. Soil Sci.* **2024**, *75*, e13507. [CrossRef]
158. Munafò, M. *Consumo Di Suolo, Dinamiche Territoriali e Servizi Ecosistemici. Edizione 2021. SNPA 22/21 [Land Consumption, Spatial Dynamics and Ecosystem Servicesibespoke. 2021 Edition. SNPA Italy 22/21]*. 2021. Available online: https://www.snpambiente.it/wp-content/uploads/2021/11/Rapporto_consumo_di_suolo_2021.pdf (accessed on 15 August 2025).
159. Assennato, F.; Di Leginio, M.; d'Antona, M.; Marinosci, I.; Congedo, L.; Riitano, N.; Luise, A.; Munafò, M. Land Degradation Assessment for Sustainable Soil Management. *Ital. J. Agron.* **2020**, *15*, 1770. [CrossRef]

Disclaimer/Publisher's Note: The statements, opinions and data contained in all publications are solely those of the individual author(s) and contributor(s) and not of MDPI and/or the editor(s). MDPI and/or the editor(s) disclaim responsibility for any injury to people or property resulting from any ideas, methods, instructions or products referred to in the content.